AD_____

Award Number: W81XWH-12-2-0038

TITLE: Prevention of Blast-Related Injuries

PRINCIPAL INVESTIGATOR: Albert I. King

CONTRACTING ORGANIZATION: Wayne State University
Detroit, MI 48202- 3692

REPORT DATE: July 2014

TYPE OF REPORT: Annual Report

PREPARED FOR: U.S. Army Medical Research and Materiel Command
Fort Detrick, Maryland 21702-5012

REPORT DOCUMENTATION PAGE

Form Approved
OMB No. 0704-0188

1. REPORT DATE	**2. REPORT TYPE**	**3. DATES COVERED**
1 Jul 2014	Annual	15 June, 2013 to 14 June, 2014

4. TITLE AND SUBTITLE
Prevention of Blast-Related Injuries

5a. CONTRACT NUMBER

5b. GRANT NUMBER
W81XWH-12-2-0038

5c. PROGRAM ELEMENT NUMBER

6. AUTHOR(S)
Albert King, John Cavanaugh, King Yang, Liying Zhang, Xin Jin, Feng Zhu

E-Mail: king@rrb.eng.wayne.edu

5d. PROJECT NUMBER

5e. TASK NUMBER

5f. WORK UNIT NUMBER

7. PERFORMING ORGANIZATION NAME(S) AND ADDRESS(ES)
Wayne State University
5700 Cass Ave., Suite 4900
Detroit, MI 48202-3692

8. PERFORMING ORGANIZATION REPORT

9. SPONSORING / MONITORING DAGENCY NAME(S) AND ADDRESS(ES)
U.S. Army Medical Research and Materiel Command
Fort Detrick, Maryland 21702-5012

10. SPONSOR/MONITOR'S ACRONYM(S)

11. SPONSOR/MONITOR'S REPORT NUMBER(S)

12. DISTRIBUTION / AVAILABILITY STATEMENT
Approved for Public Release; Distribution Unlimited

13. SUPPLEMENTARY NOTES

14. ABSTRACT This research project is designed to determine the cause of mild traumatic brain injury due to blast overpressure and, if possible, the human tolerance to blast overpressure. It consists of an experimental portion in which 12 swine and 6 post-mortem human subjects (PMHS) are to be exposed to blast. The experimental effort is supplemented by a computer modeling section which can extend the results of the tests to blast scenarios not easily achievable experimentally. In the first report, preparatory work for the proposed experiments was described along with the formulation of models of the human and swine brain subjected to blast. In this second report, results of our experimental research and of our modeling effort are presented.

15. SUBJECT TERMS
Keywords: Blast-related brain injury, Open field testing of swine and PMHS, Computer modeling of swine and human brain, brain injury mechanisms

16. SECURITY CLASSIFICATION OF:			**17. LIMITATION OF ABSTRACT**	**18. NUMBER OF PAGES**	**19a. NAME OF RESPONSIBLE PERSON**
a. REPORT	**b. ABSTRACT**	**c. THIS PAGE**			**19b. TELEPHONE NUMBER** *(include area code)*
U	U	U	UU	58	

TABLE OF CONTENTS

INTRODUCTION

This research project is designed to determine the cause of mild traumatic brain injury due to blast overpressure and, if possible, the human tolerance to blast overpressure. It consists of an experimental portion in which 12 swine and 6 post-mortem human subjects (PMHS) are to be exposed to blast. The experimental effort is supplemented by a computer modeling section which can extend the results of the tests to blast scenarios not easily achievable experimentally. In the first report, preparatory work for the proposed experiments was described along with the formulation of models of the human and swine brain subjected to blast. In this second report, results of our experimental research and of our modeling effort are presented.

STATEMENT OF WORK

The Statement of Work (SOW) for this project is as follows:

I. Perform open field blast testing on 6 anesthetized minipigs to obtain biomechanical data and on 12 anesthetized minipigs to obtain pathohistological data
II. Perform open field blast testing on 6 unembalmed post-mortem human subjects (PMHS) also known as cadavers to obtain biomechanical data
III. Develop and validate a computer model of the pig brain simulating the effects of a blast over-pressure
IV. Develop and validate a computer model of the human brain simulating the effects of a blast over-pressure

TASK I REPORT

Task I - Perform open field blast testing on 6 anesthetized minipigs to obtain biomechanical data and on 12 anesthetized minipigs to obtain pathohistological data (Original Proposal)

In this task, there were three separate work items:
1. Blast testing of instrumented swine
2. Blast testing of noninstrumented swine
3. Brain histology to assess brain injury in blast exposed swine

1. Blast Testing of Instrumented Swine

a) Test Methodology

In our plan of work, we were scheduled to perform open field blast testing of 6 anesthetized swine to obtain biomechanical data of brain response due to blast overpressure. The target incident overpressures (IOP) were nominally 150 kPa (low), 300 kPa (medium) and 450 kPa (high). Swine-related instrumentation consisted of 6

intracranial pressure (ICP) sensors inserted into various regions of the brain, 2 surface pressure sensors (SP), a triaxial linear accelerometer (LA), a triaxial angular rate sensor (AS) and 4 strain gage (SG) rosettes mounted on the swine skull. Additional instrumentation consisted of a pencil transducer mounted near the head of the swine to measure the free-field IOP and two high-speed video cameras to record the blast event. One of the cameras was focused on the head of the swine and ran at 20,000 frames/second (fps). The other provided an overall view of the blast site and ran at 10,000 fps. A Dewetron 64-channel data acquisition system was used to collect data. 1 MHz sampling rate was used for collecting SP data, 500 KHz sampling rate for ICP data, and 200 KHz sampling rate for LA, AS and SG data collection.

The ICP sensors and the SP sensors were miniature Kulite sensors that could be inserted into the brain with minimal surgery. Six ICP sensors were used in the brain. Their locations in the brain are shown in Figures 1 through 3. Figure1 is top view of the head of the pig showing the approximate locations of the frontal, parietal and center sensor. The two temporal sensors are shown in Figure 2 and the occipital sensor is shown in Figure 3. The sensors were inserted in the brain on site, in the ambulance, while other preparations were being made for the blast tests while the anesthesia level was maintained. Their precise locations in the brain are recorded and the brains have been preserved for confirmation of their locations. Upon completion of the insertion procedure, the animal was moved onto a sling for the blast experiment. However, before the test, strain gages were attached to the skull and a triaxial accelerometer package with a 3-D angular rate sensor was mounted on the skull on the occipital bone. The level of anesthesia was maintained and monitored by a veterinarian to ensure the animal felt no pain. The entire procedure on site took about 2 to 3 hours, including the hooking up of all transducers to the recording equipment, the set-up of two high speed cameras and verification of each channel. The IOP was monitored by a pencil transducer placed near the head of the test subject. It was provided by Team Wendy.

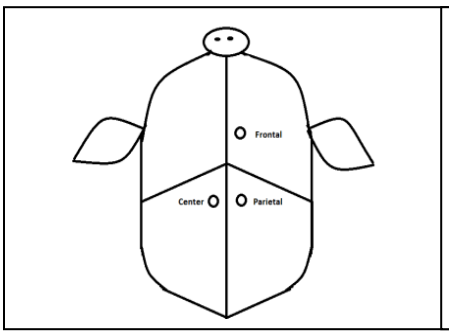

Figure 1. Top of head

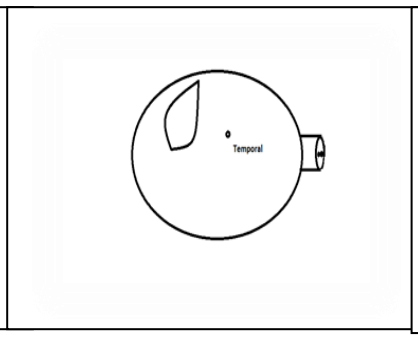

Figure 3. Side of Head

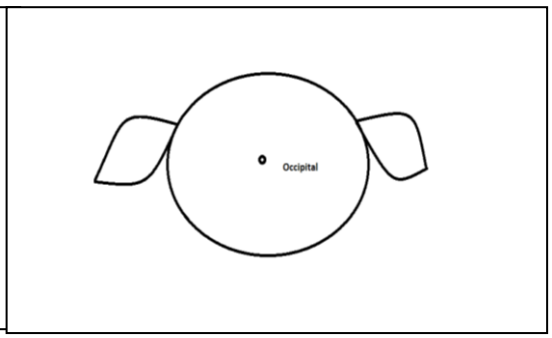

Figure 4. Rear of Head

A photograph of the test site taken during tests on an instrumented swine is shown in Figure 4.

b) Data Processing and Analysis

SP data were filtered with a 10 KHz Butterworth low pass filter. ICP, LA, AS and SG data were filtered with a 5 KHz Butterworth low pass filter. All statistical analyses were performed using DIAdem 2012 software (National Instruments Corporation, Austin, TX). All the data were grouped into three incident overpressure levels according to recorded IOP by the pencil transducer located next to the swine head. The range for the nominal low level blasts (150 kPa) is between 135 kPa to 240 kPa; while that for the nominal

Figure 4. Instrumented swine test

medium level blasts (300 kPa is between 240 kPa to 345 kPa; and that for the nominal high level blasts (450 kPa) is between 345 kPa to 480 kPa. Within each group, the pig head was oriented to the blast wave in three different directions: front, rear and side. Mean peak values of recorded data were determined for each blast level for input into the histograms.. Standard deviation and standard error were calculated for each group when the sample size was more than two. Exponential regression models were constructed to predict the relative relationship between ICP readings within groups. Resultant linear acceleration and angular rates were also calculated in each group and relationships between incident pressures and these responses were determined.

c) Results

In this reporting period, we have performed 19 blasts on three instrumented pigs. The plan was to expose each animal to three blasts in each direction and at 3 pressure

levels and to complete these nine tests in a single day. This turned out to be quite a challenge because the permissible testing time was 8 am to 4 pm with a 30-60 minute lunch break. Initially, the set up time was quite lengthy and we were unable to complete the test series for the first two animals. Thus, there were only 19 blast tests on three animals.

A summary of the instrumented pig tests are listed in Table 1, based on the previously defined nominal IOPs.

Table 1: Summary of Tests on Instrumented Pigs

	Low IOP	Medium IOP	High IOP
Front	2	4	4
Rear	2	2	2
Side	1	1	1

For each test a summary of peak values is listed below (Tables 2, 3 and 4). Some data points were lost due to sensor malfunctioning and are left blank in the tables. The relationships between IOP and ICP, LA and AS data are illustrated in Figures 5-9. With higher IOPs, ICP increased in different regions of the brain. For frontal blasts, among all the regions of the brain, ICP readings in the parietal region had the highest values at medium and high IOP levels, as shown in Figure 5. ICP readings in the central region of the brain were much lower than those in the parietal region. For frontal blasts, frontal SP readings were higher than those in the occipital region. In rear blasts, all the ICP readings at different regions increased with increases in IOP, as shown in Figure 6. ICP readings in the parietal region had the highest values among all the measured ICPs. SP readings at the occiput were higher than frontal SP readings. In side blasts, only one set of data were acquired. All the ICP readings increased as IOP increased (Figure 7).

Resultant linear head accelerations increased with increases in IOP in frontal, rear and side-on blast exposures of the head with some exceptions (Figure 8). More resultant angular rate data are required to determine trends (Figure 9).

Table 2: Summary of ICP Peak Values

Test date	Blast No.	Test ID	Pencil Pressure	Orientation	Frontal	Parietal	Left Temporal	Right Temporal	Occipital	Center
10/11/2013	1	5	253.4	Front	151.3	179	193.7	187.6	166.3	148.7
10/29/2013	2	12	150.3	Front	131	158.7	142.8	147.9	121.6	147.8
9/24/2013	1	1	223.5	Front	174.5	543.3	288.9	174.1		163.9
9/24/2013	2	2	260.5	Front	211.9	575.3	325	238.4		238.1
10/11/2013	2	6	324.2	Front	304.8	584.9	432.7	482.9	357	243.3
10/29/2013	1	11	285.5	Front	225.4	224.1	205.5	211.6	203.5	174.4
9/24/2013	3	3	385.0	Front		938.6		301.1		335.1
9/24/2013	4	4	464.7	Front		956.8		1710.7		350.6
10/11/2013	3	7	413.7	Front	373.7	677.6	398.7		407.6	265.5
10/29/2013	3	13	460.6	Front	233.7	414.6	374	338.4	360.6	287.9
10/11/2013	4	8	148.2	Rear	80	105	68.4		70.5	55.6
10/29/2013	4	14	149.6	Rear	51.2	47.9	29.1	39.1	41.8	66.3
10/11/2013	5	9	280.6	Rear	148.6	347	130.1		146	82.7
10/29/2013	5	15	302.7	Rear	62.3	77.9	54.4	52	86.6	32.2
10/11/2013	6	10	345.4	Rear	234.4	248	280.7		178.4	120.6
10/29/2013	6	16	413.7	Rear	113.4	175.2	45.4	63.7	91.4	31.9
10/29/2013	9	19	150.3	Side	55.4	61.9	38.2	64.6	84.9	27.1
10/29/2013	8	18	264.8	Side	121.6	74.6	56.2	72.3	235.6	41.2
10/29/2013	7	17	421.3	Side	139.3	109.3	88.6	77.9	273.1	134.1

Table 3: Summary of Head Surface Pressure (SP) Peak Values

			Incident (kPa)	Surface Pressure (kPa)	
Test date	Blast No.	Test ID	Pencil Pressure	Frontal	Occipital
10/11/2013	1	5	253.4	229.2	122.6
10/29/2013	2	12	150.3	24.8	127.6
9/24/2013	1	1	223.5	409.6	3229.4
9/24/2013	2	2	260.5	467.6	252.1
10/11/2013	2	6	324.2	236.1	378.9
10/29/2013	1	11	285.5	36.2	187.8
9/24/2013	3	3	385.0	1272.1	1647.9
9/24/2013	4	4	464.7	468	3830.7
10/11/2013	3	7	413.7	414.8	2125.8
10/29/2013	3	13	460.6	61.5	307.2
10/11/2013	4	8	148.2	61.1	2610.8
10/29/2013	4	14	149.6	18.3	128.5
10/11/2013	5	9	280.6	105.2	754.6
10/29/2013	5	15	302.7	29.3	237.5
10/11/2013	6	10	345.4	66.5	2794.5
10/29/2013	6	16	413.7	32.5	288.3
10/29/2013	9	19	150.3	21.3	19.2
10/29/2013	8	18	264.8	36.8	56.4
10/29/2013	7	17	421.3	55.5	100.8

Table 4: Summary of Head Linear Acceleration and Angular Rate Response

			Incident (kPa)	Orientation	Linear Head Accelerations (g)	Angular Head Velocities (rad/s)
Test date	Blast No.	Test ID	Pencil Pressure	Orientation	Resultant	Resultant
10/11/2013	1	5	253.4	Front		
10/29/2013	2	12	150.3	Front	344.5	30
9/24/2013	1	1	223.5	Front	175.3	
9/24/2013	2	2	260.5	Front	295.2	
10/11/2013	2	6	324.2	Front		
10/29/2013	1	11	285.5	Front	446.5	470.3
9/24/2013	3	3	385.0	Front	503.6	
9/24/2013	4	4	464.7	Front	536	
10/11/2013	3	7	413.7	Front		
10/29/2013	3	13	460.6	Front	635.6	1330.2
10/11/2013	4	8	148.2	Rear	188.8	13.5
10/29/2013	4	14	149.6	Rear	204.2	13.2
10/11/2013	5	9	280.6	Rear	383.1	76.2
10/29/2013	5	15	302.7	Rear	275.9	37.6
10/11/2013	6	10	345.4	Rear	515	148
10/29/2013	6	16	413.7	Rear	430.7	30.6
10/29/2013	9	19	150.3	Side	249.4	21.3
10/29/2013	8	18	264.8	Side	439.6	46.1
10/29/2013	7	17	421.3	Side	444.9	44.6

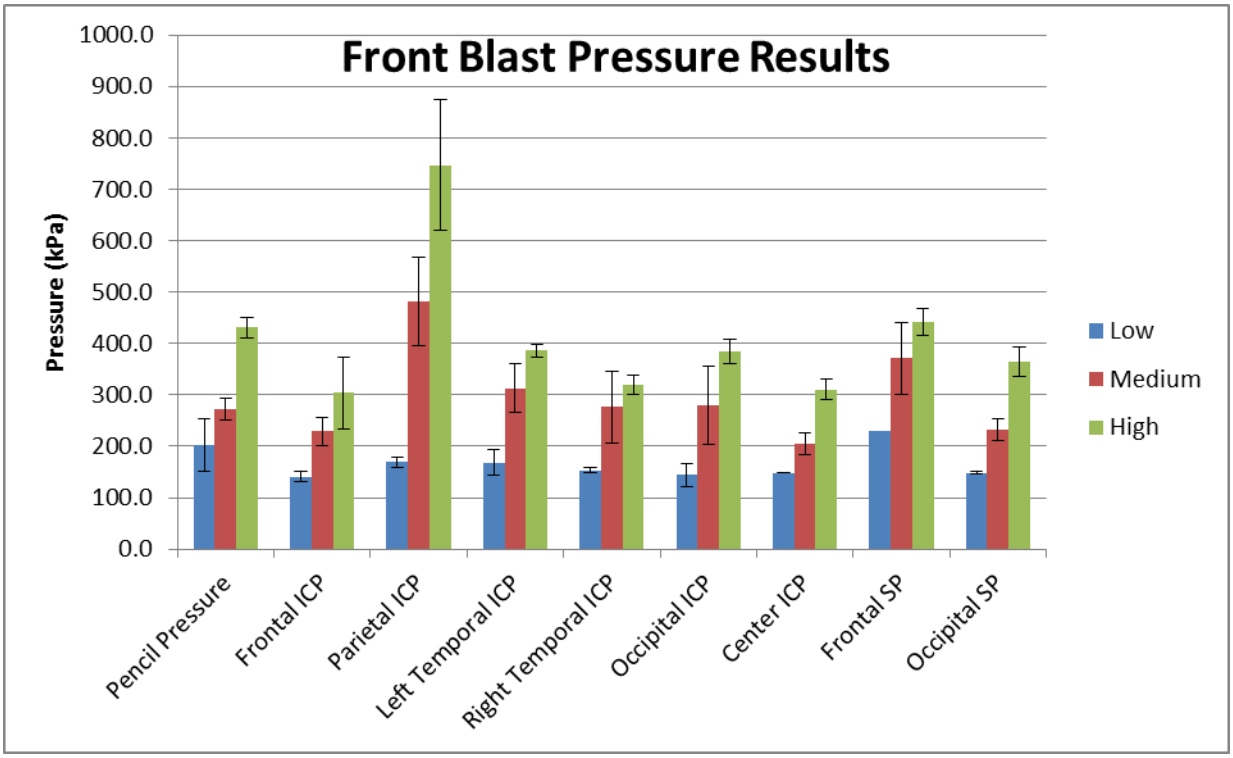

Figure 5: Pressure results in front direction blasts

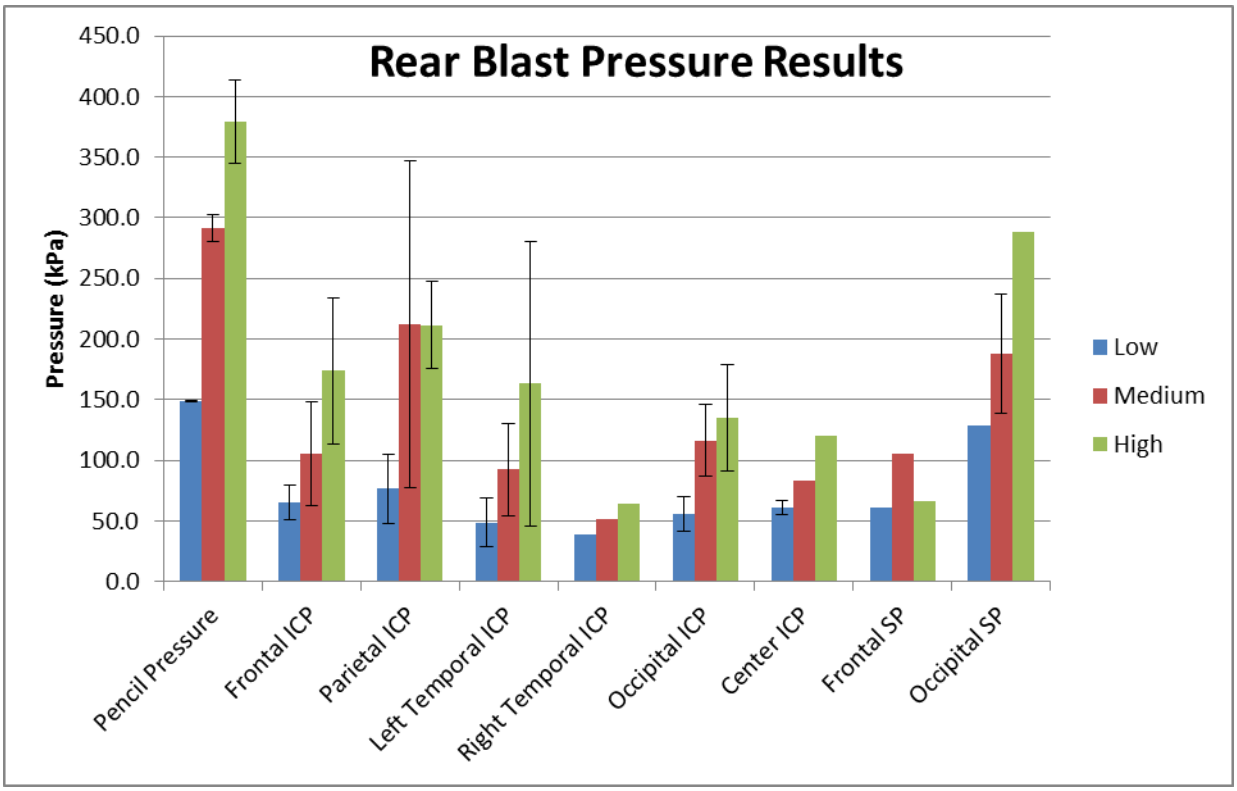

Figure 6: Pressure results for rear blasts

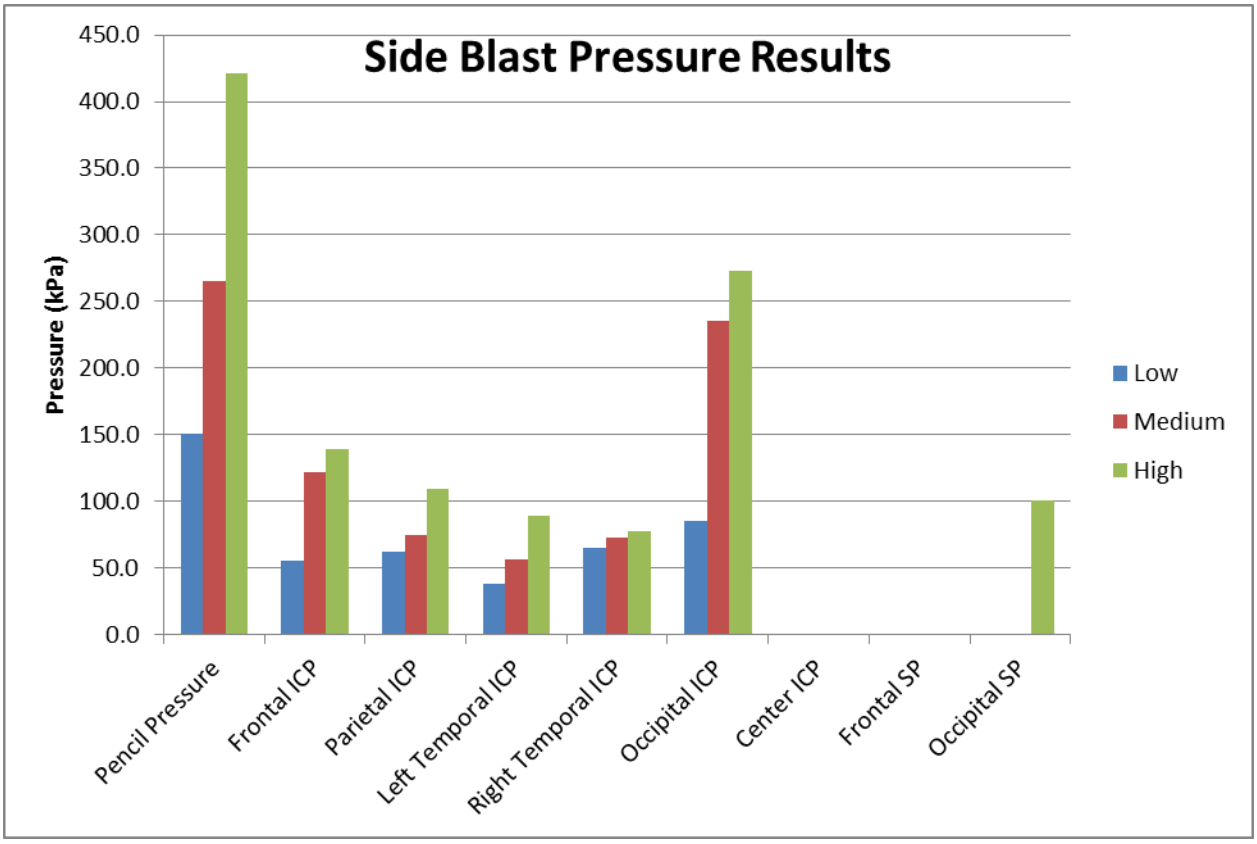

Figure 7: Pressure results for side blasts

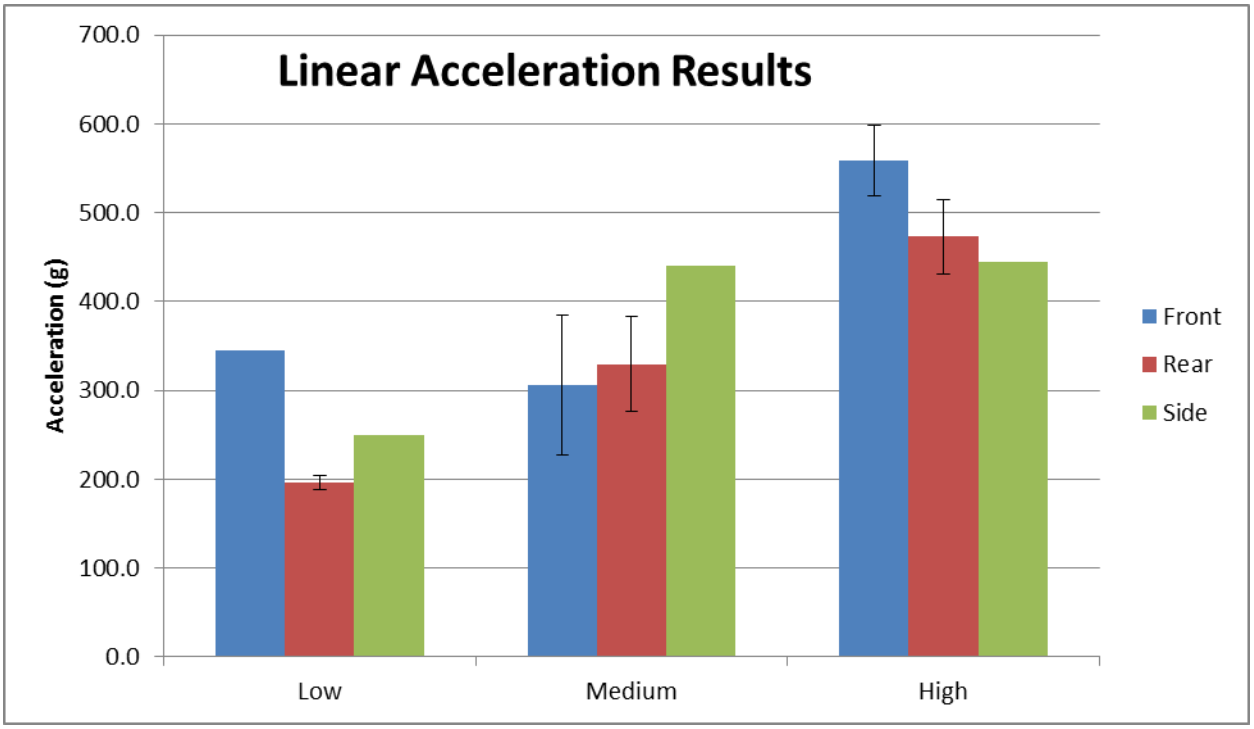

Figure 8: Resultant linear head acceleration results

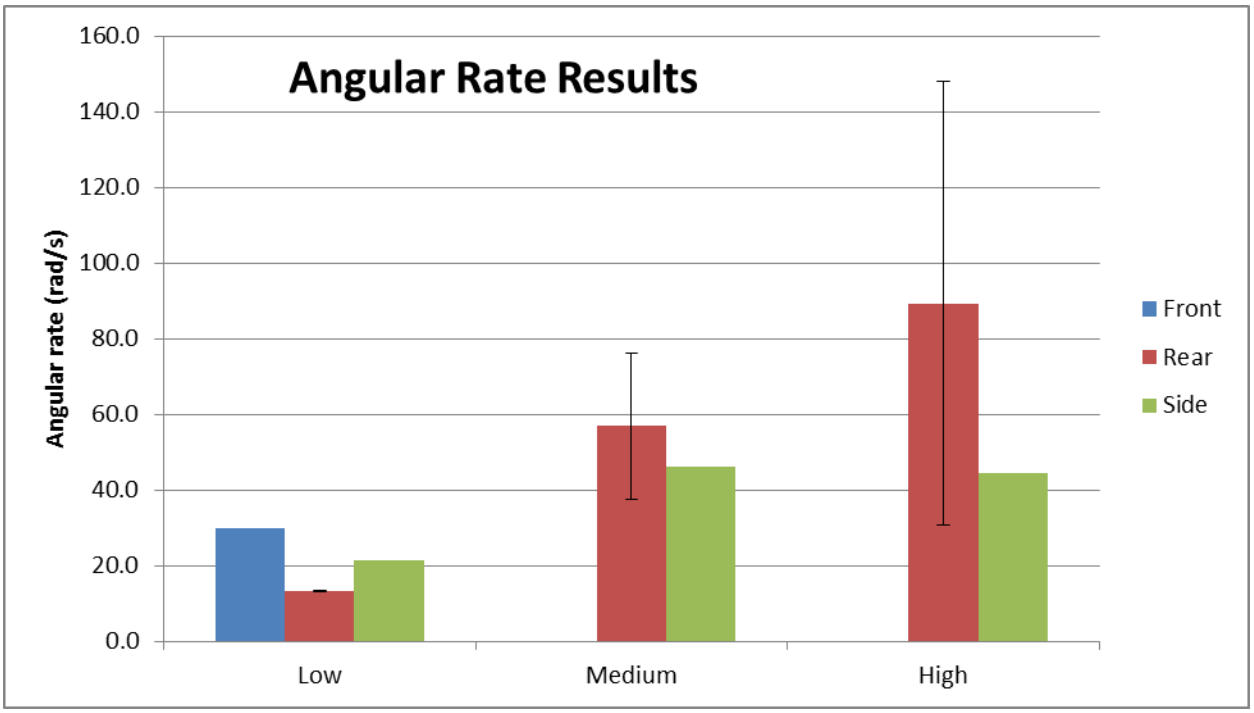

Figure 9: Resultant head angular velocity results

Scatter plots of ICP readings for each blast direction are plotted in Figures 10 15 the various brain regions, along with the exponential equations which best fit these data. These plots illustrate the relationship between IOP and ICP. The largest sample size is for frontal blasts.

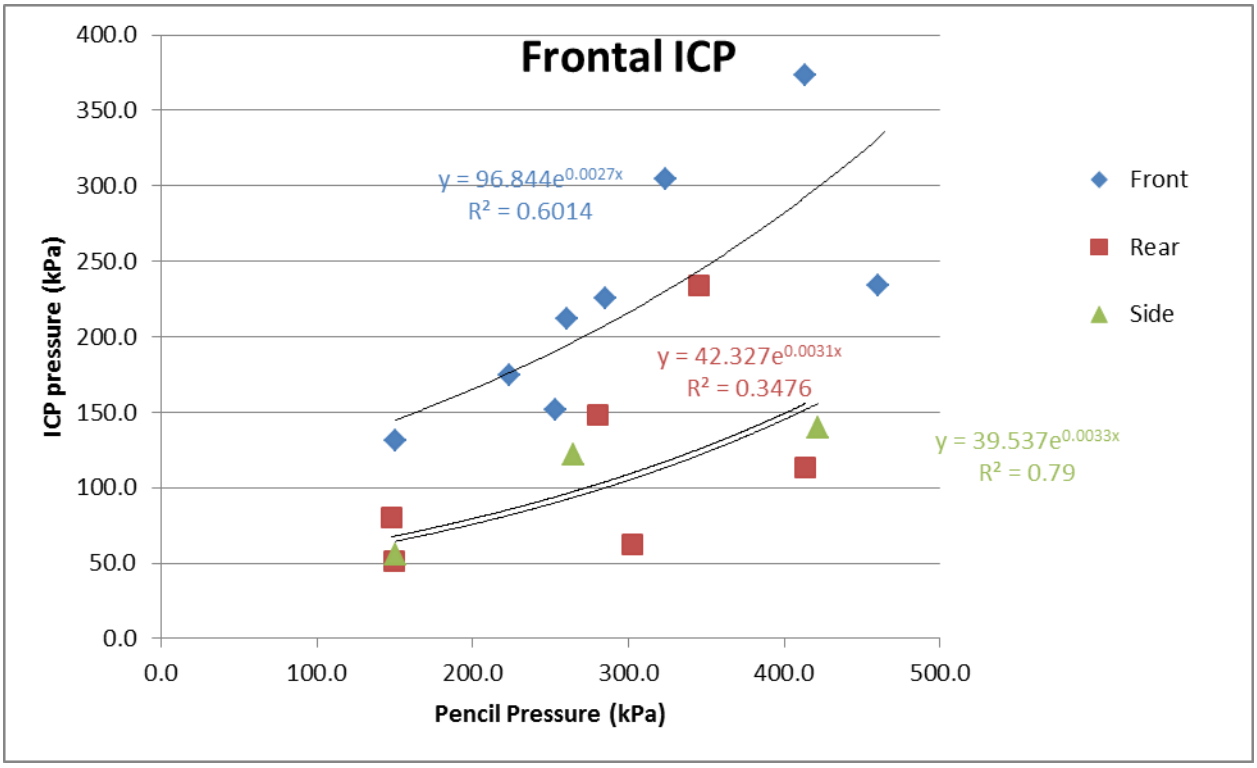

Figure 10. IOP vs. ICP in the frontal brain region

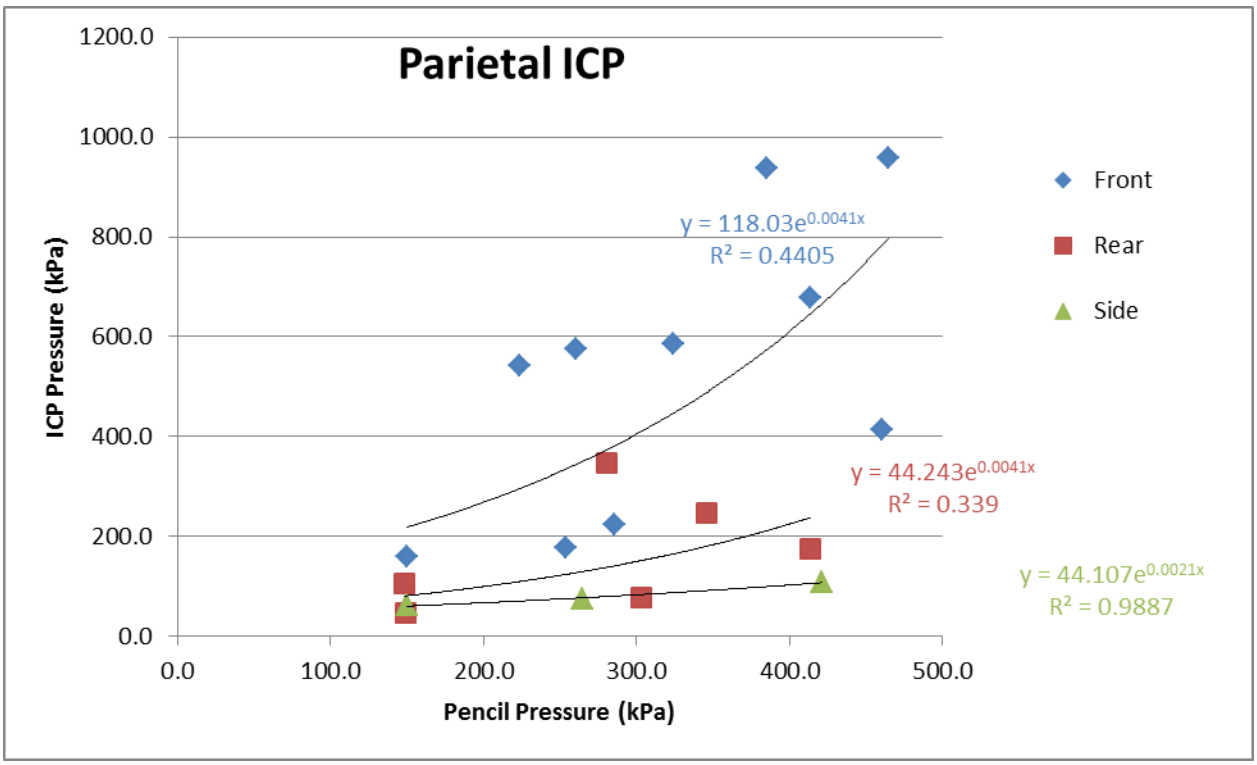

Figure 11. IOP vs ICP in the parietal brain region

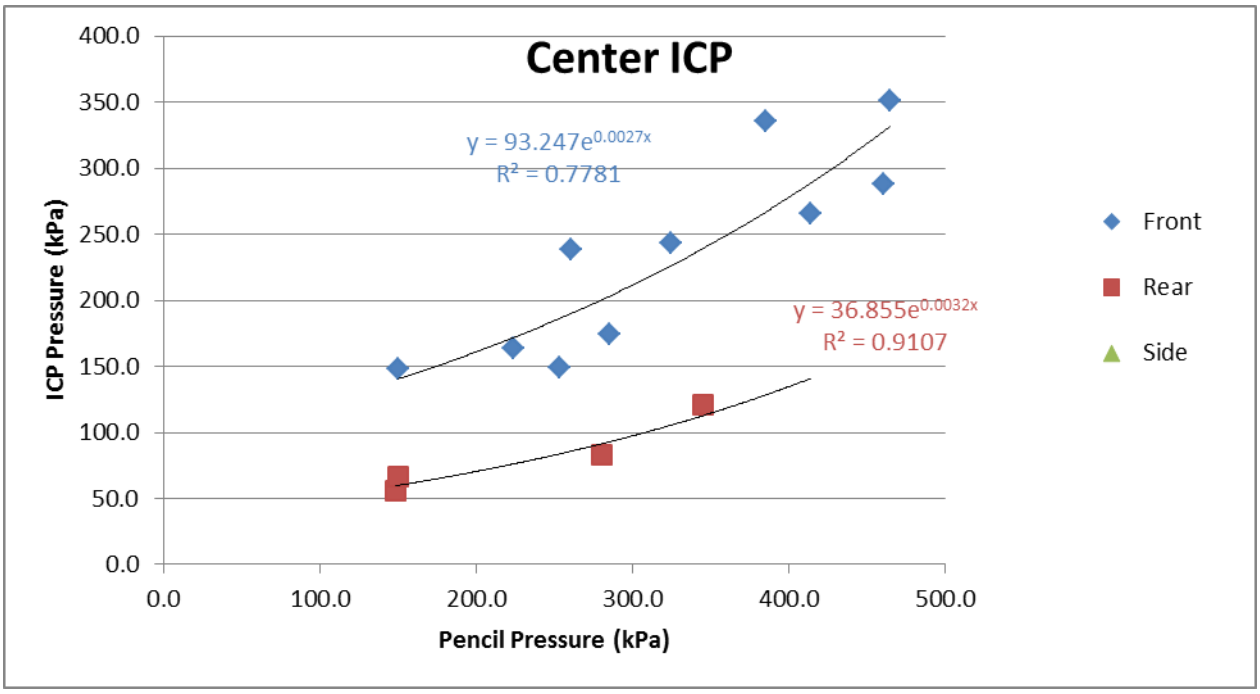

Figure 12. IOP vs ICP in the central brain region

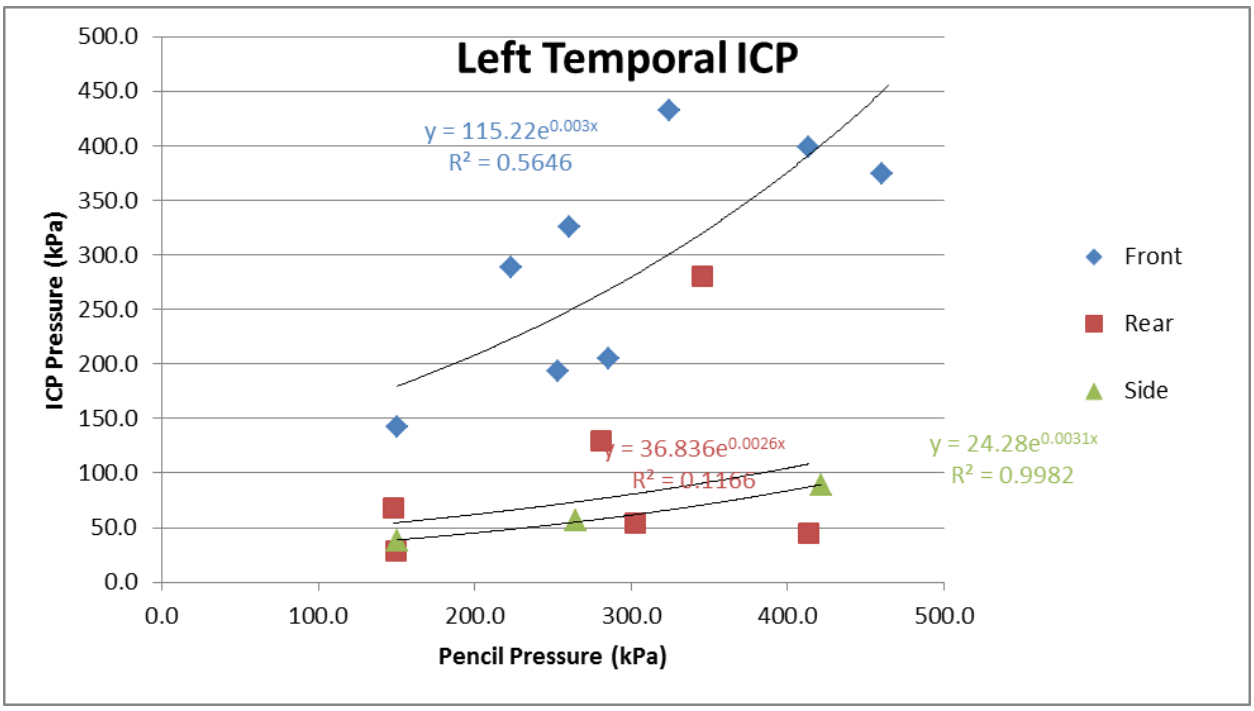

Figure 13, IOP vs ICP in the left temporal region

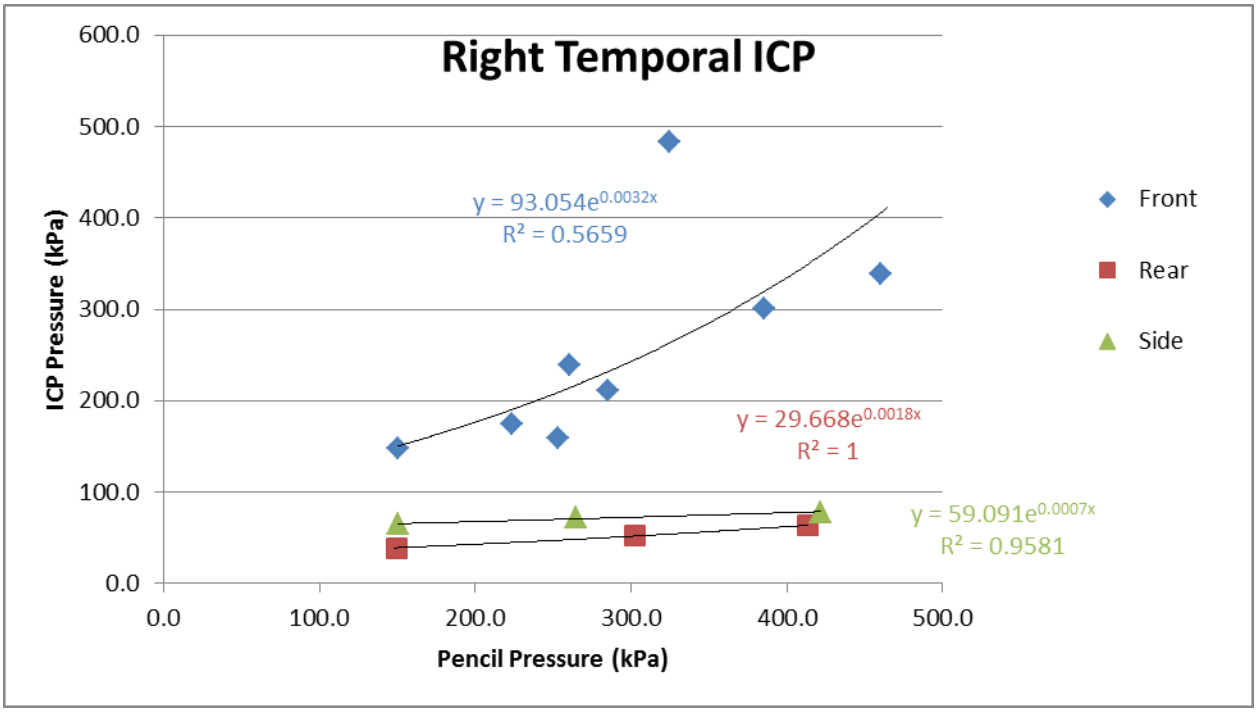

Figure 14, IOP vs ICP in the right temporal region

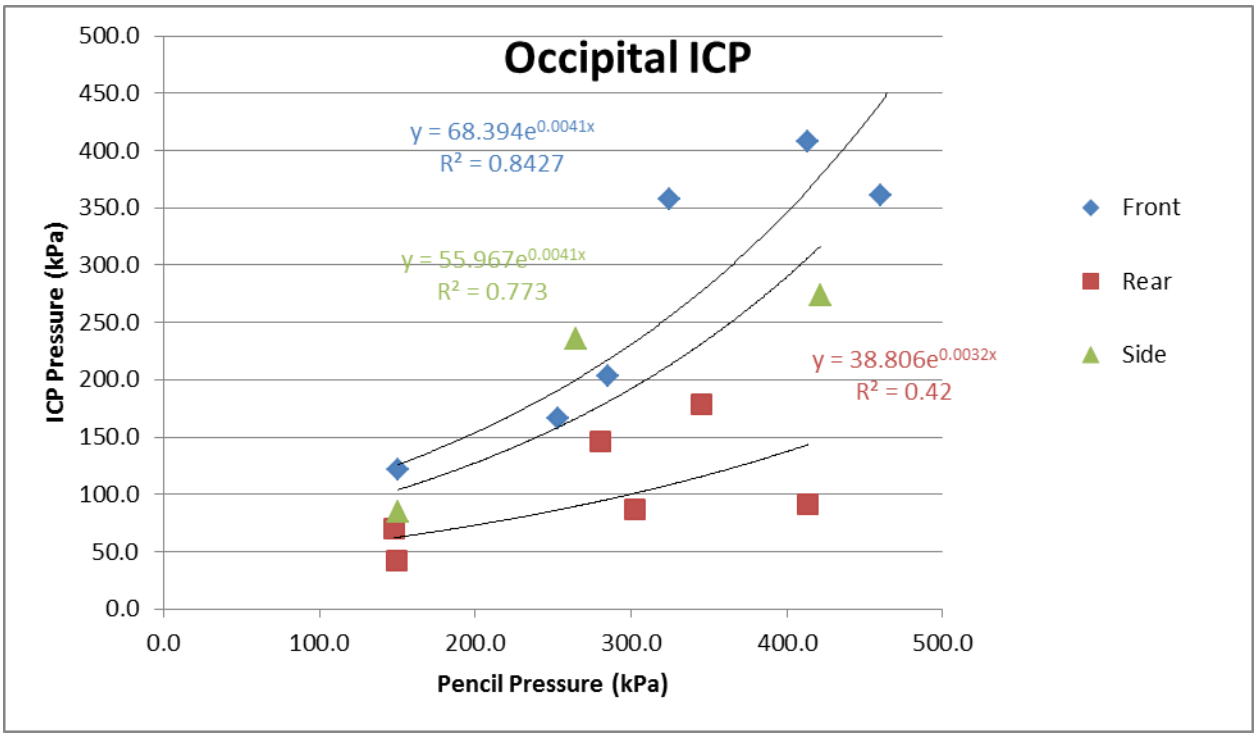

Figure 15. IOP vs ICP in the occipital region

In Figures 16 and 17, linear acceleration and angular velocity are plotted against IOP. Linear acceleration tends to increase with increasing IOP. However, there is no correlation of angular acceleration with IOP..

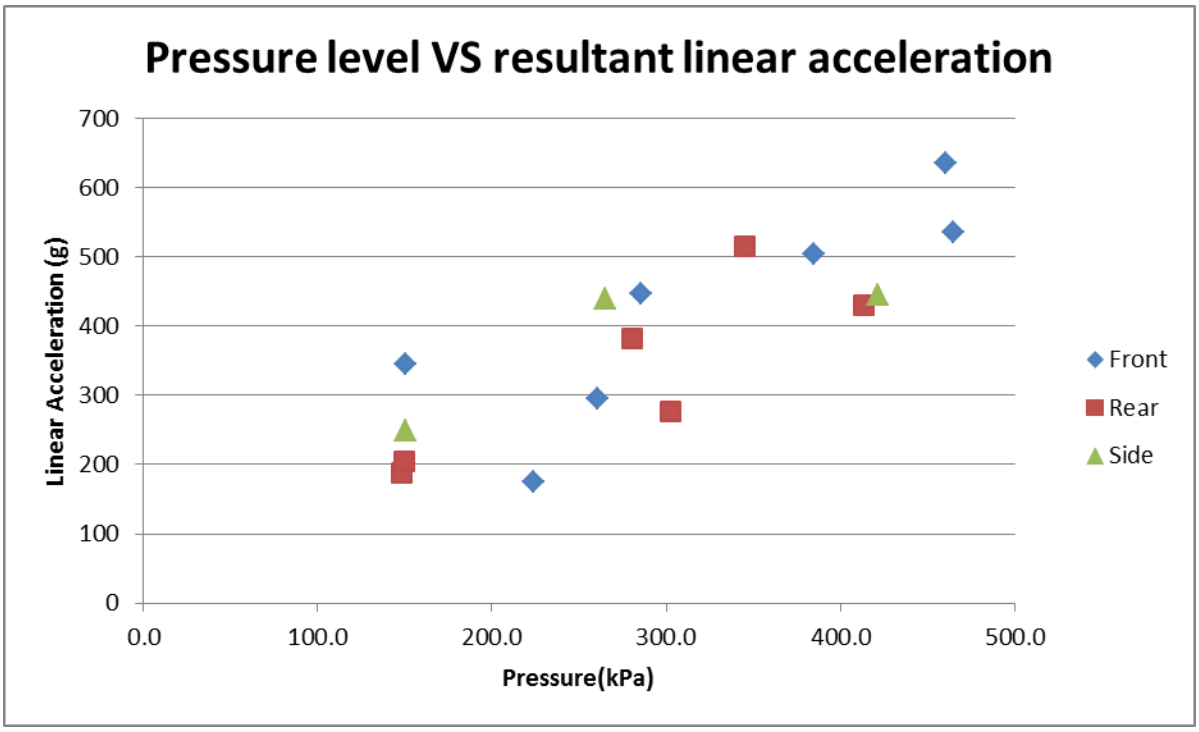

Figure 16. Resultant linear acceleration as a function of IOP

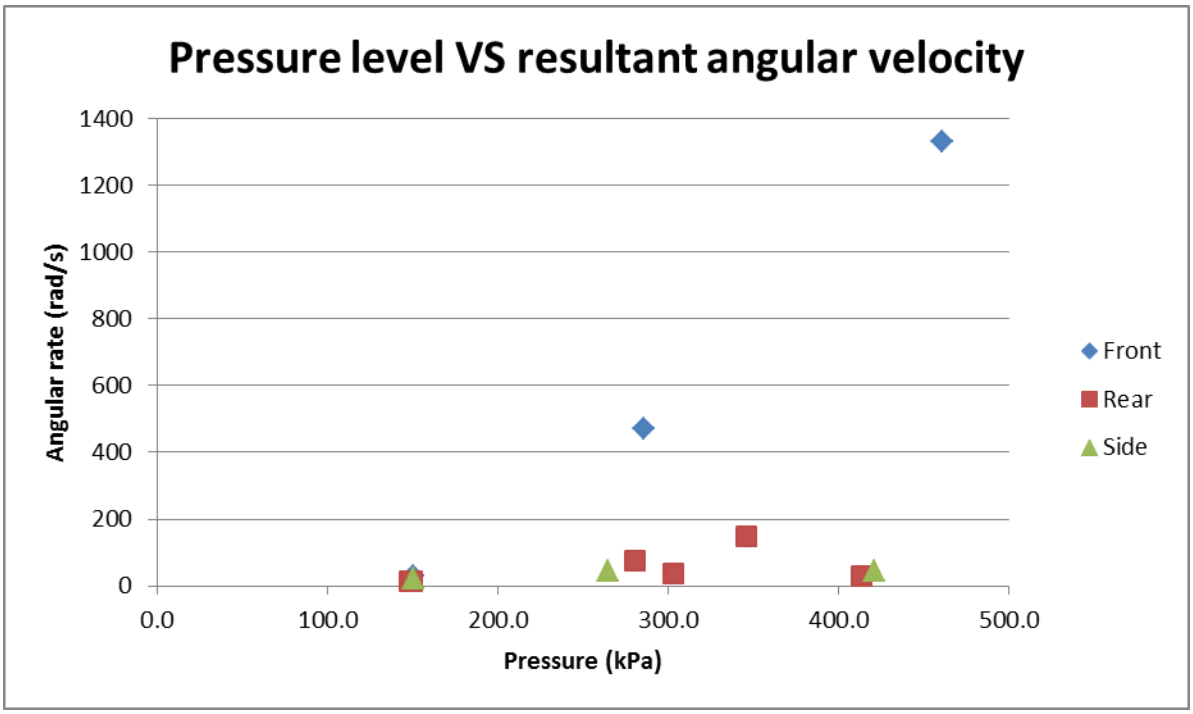

Figure 17. Resultant angular velocity as a function of IOP

High linear acceleration is associated with primary blast, as shown in Figures 8 and 16. However, the duration of the acceleration is relatively short, as shown in Table 5. This high acceleration is due to the pressure differential experienced by the head when the leading edge of the blast or shock wave reaches the head. There is high pressure on the leading edge and ambient pressure on the other side of the head, the trailing edge. Thus, a force is generated to move the head in the direction of the motion of the shock wave. Thus, in primary blast, the head does undergo motion when the shock wave goes by it. In fact, the head acceleration due to the blast wind or tertiary blast is not significant.

Table 5. Linear Acceleration and Angular Velocity Durations due to Primary Blast

Test Date	Frontal Blast	Linear Acceleration Duration (ms)	Angular Velocity Duration (ms)
24-Sep	1	0.25	0.22
	2	0.38	0.2
	3	0.35	0.26
	4	0.34	0.2
11-Oct	1	0.25	0.66
	2	0.33	0.24
	3	0.25	0.39
29-Oct	1	0.36	0.36
	2	0.38	0.49
	3	0.38	0.4
Test Date	Rear Blast	Linear Acceleration Duration (ms)	Angular Velocity Duration (ms)
11-Oct	4	0.34	0.54
	5	0.32	0.58
	6	0.3	0.54
29-Oct	4	0.34	0.7
	5	0.34	0.51
	6	0.41	0.8
Test Date	Rear Blast	Linear Acceleration Duration (ms)	Angular Velocity Duration (ms)
29-Oct	7	0.38	0.6
	8	0.71	0.53
	9	0.73	0.33
	Average	0.38	0.45

Figure 18 shows the relationship between ICP and head linear acceleration and angular velocity. The arrival of the ICP wave is almost simultaneous with motion and thus the motion is due to the primary wave. There is a slight increase in linear acceleration and angular velocity at 7.5 ms due to the arrival of the blast wind but the magnitudes are much lower than those due to primary blast.

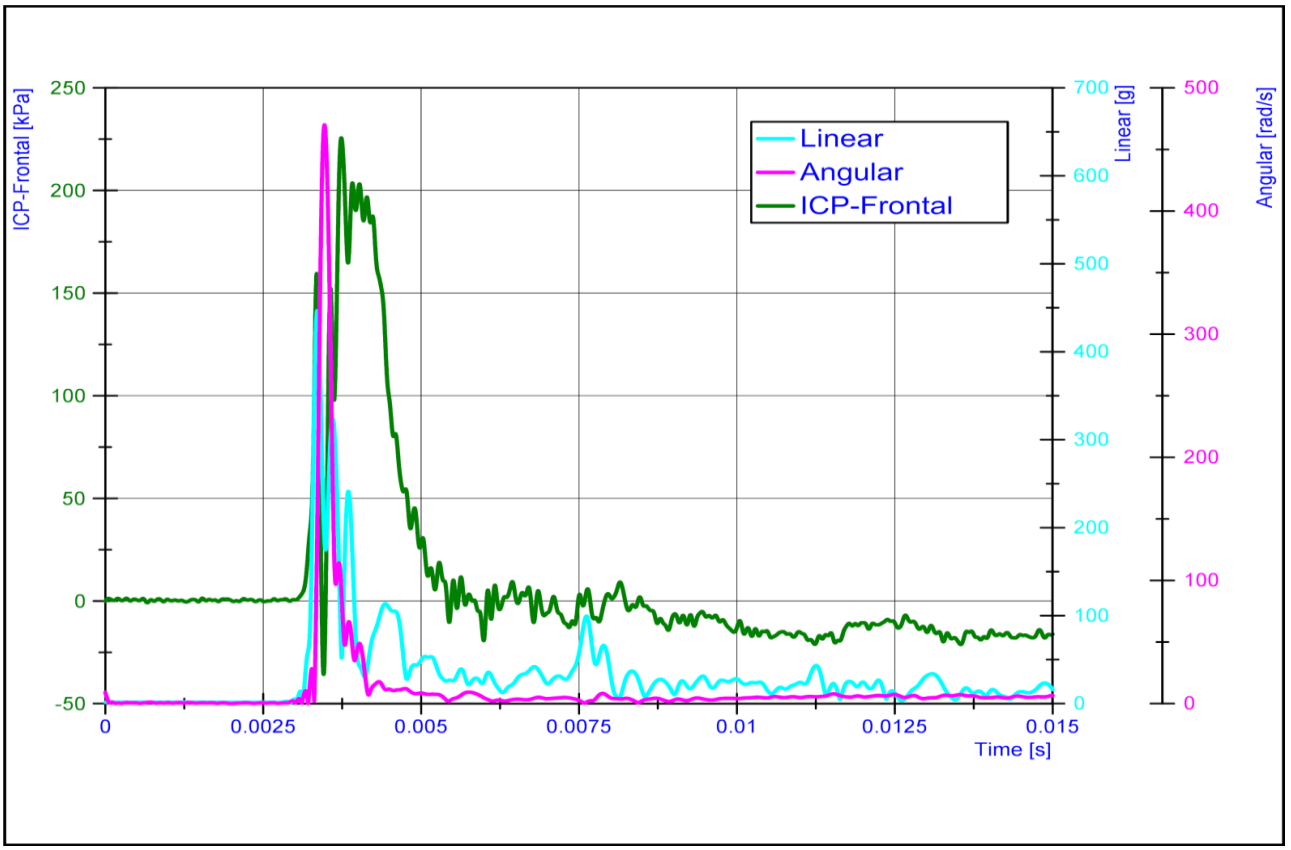

Figure 18. Relationship between ICP and head motion (head linear acceleration and angular velocity) demonstrates that primary blast imparts a severe acceleration to the head, albeit the duration is very short

2. Blast Testing of Non-Instrumented Swine

Test Methodology

The non-instrumented swine were exposed to a single blast to assess the injuries sustained. Thus, the test methodology is as follows:

The animal was anesthetized at Wayne State University and transported in an ambulance to the test site on the day of the experiment, arriving at about 8 am, after a 90-120 minute drive from Detroit, MI to Port Clinton, OH. Anesthesia levels were maintained until it is ready for testing. The wait was due to the time needed to prepare the instrumented swine or cadaver which was to be tested alongside the non-instrumented swine. So for the first test of the day, there were generally two test subjects exposed to the same blast. In ine case, the noninstrumented swine was tested alone. After the non-instrumented swine was exposed to blast, it was taken back into the ambulance and driven back to Wayne State University for observation and blood draw. It was sacrificed on the third day and the brain was removed and preserved for histological study.

The experimental protocol calls for the testing of 12 swine at two pressure levels –six at 300 kPa and 6 at 450 kPa, nominally. The protocol also included 6 sham animals which underwent the entire test protocol but were not exposed to blast. That is, the sham animals were anesthetized, transported by ambulance to Ohio where they waited for about 2 hours, put in the sling used to test blast animals for about 45 minutes, returned to the ambulance and driven back to Wayne State University for observation and blood draw. They were sacrificed on the third day and the brain was removed and preserved for histological study.

3 Brain histology to assess brain injury in blast exposed swine

Brain Material Available

During this period, a total of 5 blasted swine brains and 4 sham swine brains were obtained for assessing the effects of open field blast overpressure by various histological methods. Table 6 shows the test dates and the exposed pressures. Furthermore, blood was collected at various time points for subsequent temporal assessment of the serum for various injury biomarkers. Biomarker analyses allows for additional correlations with histological outcome performed at the terminal survival point of 72 hours.

A multitude of histologoical techniques have been developed to assess blast induced neurotrauma on these brains. Axonal injury will be assessed by beta amyloid precursor protein and neurofilament light chain immunocytochemistry and by silver staining. Inflammatory response will be assessed by glial fibrillary acidic protein (GFAP) and microglial (Iba1) immunocytochemistry. Cell injury will be assessed by caspase 3 immunocytochemistry, FluoroJade B, TUNEL and H&E staining. Additionally, the presence of hemorrhage will be assessed by Prussian blue staining.

Serum harvested at the stated time points (Table 6) will be assessed for temporal changes in various biomarkers (S100B, NSE, MBP, NF-H, SBDP, IL-6, HSP-70).

Table 6. Details of Blast and Sham Tests for Histological Studies of Blast-Iinduced Neurotrauma

					Blood Collection Time Points							
Test Date	Blast #	Test ID	Pencil Pressure (kPa)	Pencil Pressure (psi)	Pre-Blast	6 Hours	24 Hours	48 Hours	72 Hours	Date of Perfusion	Histology	Biomarkers
9-24-13	1	Uninstrumented 1	224	32.49	9-24-13	9-24-13	9-25-13	9-26-13	9-27-13	9-27-13	√	√
10-22-13	2	Sham 1	sham	sham	10-22-13	10-22-13	10-23-13	10-24-13	10-25-13	10-25-13	√	√
11-5-13	3	Uninstrumented 2	332	48.15	11-5-13	11-5-13	11-6-13	11-7-13	11-8-13	11-8-13	√	√
11-5-13	4	Uninstrumented 3	305	44.24	11-5-13	11-5-13	11-6-13	11-7-13	11-8-13	11-8-13	√	√
11-19-13	5	Sham 2 (True)	sham	sham	11-19-13	11-19-13	11-20-13	11-21-13	11-22-13	11-22-13	√	√
11-19-13	6	Sham 3 (True)	sham	sham	11-19-13	11-19-13	11-20-13	11-21-13	11-22-13	11-22-13	√	√
12-9-13	7	Uninstrumented 4	222	32.2	12-9-13	12-9-13	12-10-13	12-11-13	12-12-13	12-12-13	√	√
12-9-13	8	Uninsturmented 5	263	38.14	12-9-13	12-9-13	12-10-13	12-11-13	12-12-13	12-12-13	√	√
12-10-13	9	Sham 4 (True)	sham	sham	12-10-13	12-10-13	12-11-13	12-12-13	12-13-13	12-13-13	√	√

Technique to section the brain:

Our efforts in cutting swine brain into blocks of tissue and further into 40-µm thick serial sections have evolved from a hand-made paraffin brain mold to a prototype brain slicer matrix for Yucatan swine brain to the currently used custom made brain matrix (Zivic Instruments), as shown in Figure 19 The current brain slicer enables cutting of the brain into 5 mm thick blocks which are further sectioned to 40 µm thick serial sections that are stained by various histochemical and immunohistochemical techniques. Thus far we have sectioned 2 blocks each from all 5 blast swine brains and 4 sham brains. Currently, we are in the process of sectioning block 3 from all these brain which is anticipated to be complete by July 2014.

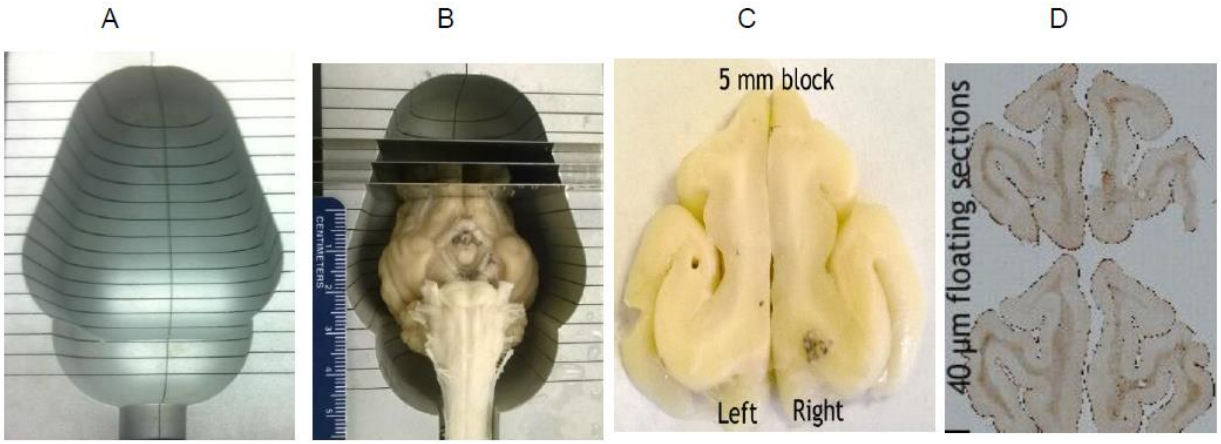

Figure 19 A. Top view of the brain matrix mold. B. The mold with a swine brain in it and with blades positioned to obtain a block. C. A representative 5–mm block obtained from the brain. D. A representative 40-µm thick section

Developing a reliable immunohistochemical (NF-L and β-APP) and silver staining technique to assess axonal injury from swine brain sections

We were able to standardize the immunohistochemical technique to visualize axonal injury in blast and sham treated brain sections. As part of our efforts, 40-µm thick representative serial sections from two 5 mm blocks of brain tissues exposed to sham (n=4 animals) and blast (n=5 animals) have been processed by incubating them in antibodies directed against neurofilament (NF-L) light chain and beta amyloid precursor protein (β-APP) (Figure 20). The sections were further developed by avidin biotin peroxidase reactivity. Further observation of NF-L stained sections revealed presence of well stained cell bodies with their apical dendrites as well as stained axons with vacuolations and swellings in the white matter tract. Immunostaining with β-APP also revealed specifically swollen axons, axons with retraction bulbs, and axons with beaded appearance in the white matter. Furthermore, there appears to be a preponderance of β-APP reactive axonal profiles in sections from blast exposed brain sections than in sham sections. Both NF-L and β-APP immunohistochemistry are routinely used to assess axonal injury following brain injury. Currently, our efforts are directed at quantifying the extent of these axonal injury changes as revealed by both NF-L and β-APP immunohistochemistry. In addition to immunohistochemical staining, we also stained representative sections with a silver impregnation technique (Figure 20) that revealed degenerating axons in white matter tracts from these prefrontal cortical regions.

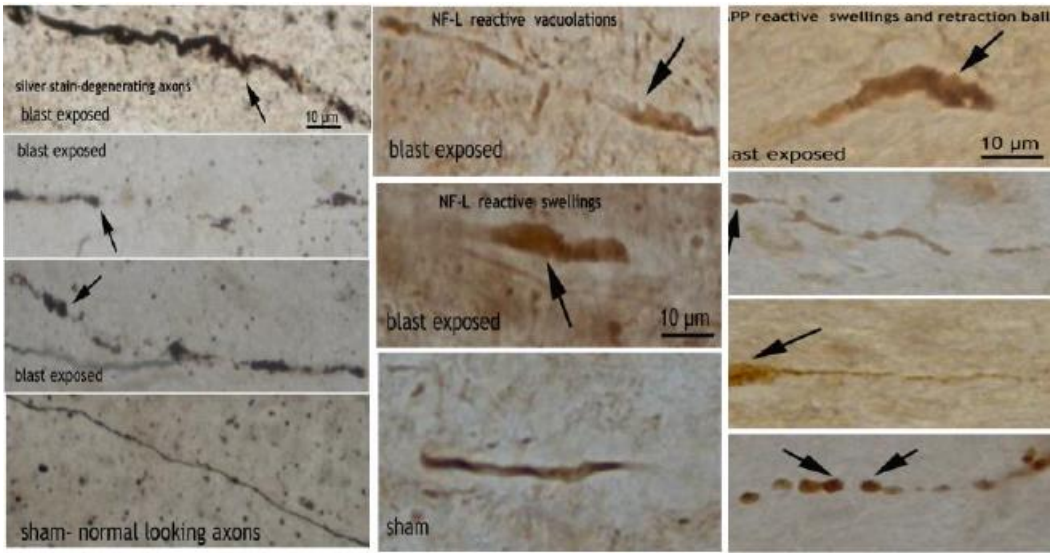

Figure 20. Brain regions from blast and sham exposed sections stained by NF-L and β-APP immunohistochemistry.

Developing a reliable immunohistochemical and quantification technique to assess astrocyte proliferation

During this period we were also able to establish a reliable staining procedure to assess astrocytic proliferation. For this purpose, representative sections from blocks 1 and 2 of all 9 swine brains (blast =5; sham =4) were incubated overnight in a mouse anti glial fibrillary acidic protein (GFAP) cocktail (cat # NE1015, Calbiochem), and then developed by avidin biotin peroxidase reactivity. Observation of these sections under light microscope revealed well stained astrocytes (Figure 21) in both white and grey matter regions with indication of high astrocytic proliferation in blast exposed swine sections.

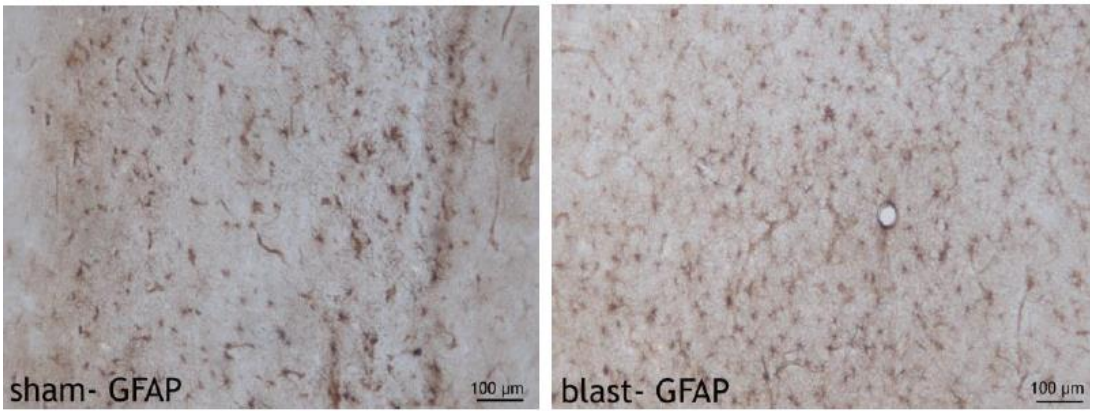

Figure 21. Astrocytic activity in regions from blast and sham exposed sections stained by GFAP immunohistochemistry.

Development of a quantification technique to assess the extent of astrocytosis

All stained sections were imaged using our newly procured automatic Surveyor Software. First, each section was completely scanned at x5 magnification to give a panoramic image of the whole section. Then representative images (x10) were obtained to perform a preliminary quantification of the number of astrocytes in each image (20 images per brain; blast 5x20 = 100 images; sham 4x20 = 80 images). For this purpose, each image was inverted (Figure 22) using the invert option in ImageJ software and the number of astrocytes was counted using the cell counter function in ImageJ.

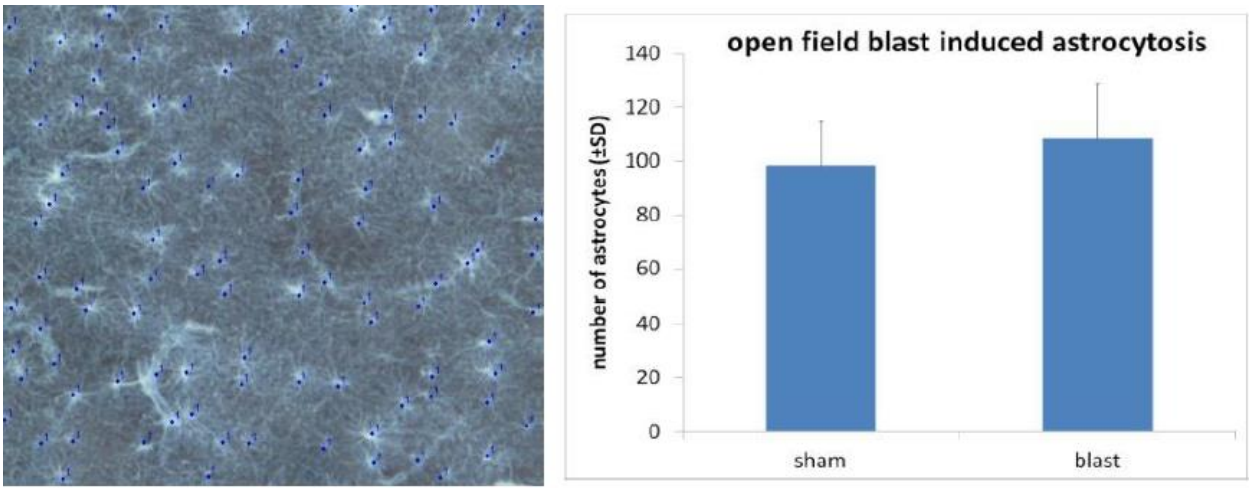

Figure 22. An inverted image showing the counted astrocytes indicated by the blue dots. The histogram showing the preliminary astrocyte counts from sham and blast exposed sections.

This preliminary quantification suggests enhanced astrocytic proliferation in blast group than in sham group (Figure 4) and needs further validation. In addition, we are also working towards developing a technique to maintain consistency in obtaining images of GFAP stained areas. For this purpose, the entire section will be scanned by the Surveyor at x5 magnification to obtain a panoramic image. Then using a measurement tool in the Surveyor Software, the average length of the white matter track will be determined. Then representative x10 images will be taken at equidistant points (each point approximately 5 mm apart) throughout the white matter, thereby fixing 5 specific points along the track in each hemisphere for each section. This allows for each section to be imaged in the same location given a fixed starting point to measure from. This technique eliminates any ambiguity while quantifying using ImageJ, as opposed to imaging randomly selected regions along that white matter tract. Moreover, it allows the quantitative analysis to be far more accurate since identical regions are studied for each test subject.

<u>Developing a reliable immunohistochemical technique to assess microglial proliferation</u>

This period also saw the development of a reliable immunohistochemical staining technique to assess microglial proliferation. For this purpose, representative sections from blocks 1 and 2 of all 9 swine brains (blast =5; sham =4) were incubated overnight in a rabbit anti Iba1 antibody (cat # 019-19741, Wako Chemicals) and then developed by avidin biotin peroxidase reactivity. Observation of these sections under light microscope revealed well stained microglia (Figure 23) in both blast and sham exposed swine sections. Our preliminary observations also revealed potential areas of microglial clustering in white matter tracts and we are working on a preliminary quantification technique to assess the differences in this clustering. Areas of with microglial clusters may indicate potential site of injury as they cluster to remove cellular debris.

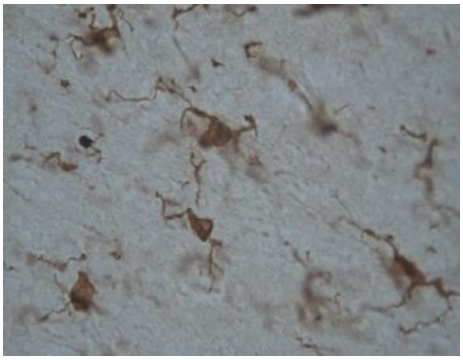

Figure 23. Iba1 stained microglia in a blast exposed swine brain section

Development of a staining technique to assess apoptosis

Our initial efforts are directed at staining 40 µm brain sections from blast and sham brains by incubating them in anti Cleaved Caspase-3 (Asp175) antibody and further incubation in an appropriate secondary antibody followed by routine avidin biotin peroxidase technique. Our initial results although indicate areas of cleaved caspase reactivity, their specificity in the cortical neurons still needs to be established. As part of this effort to assess neurons undergoing apoptosis, we are developing a double label immunofluoroscence staining technique by incubating sets of brain sections in anti-Cleaved Caspase-3 antibody as well as in anti Neuronal Nuclei (NeuN) antibodies. The sections were further incubated in secondary antibodies tagged with Dylight 488 (cleaved caspase) and AMCA (NeuN). In the image shown in Figure 24 blue indicates NeuN staining and green indicates cleaved caspase staining Our current efforts are directed at optimizing this staining technique for better visualization of cells undergoing apoptosis using the single labeling (immunohistochemistry using anti cleaved caspase antibodies alone) as well as dual labeling (immunofluorescence: anti cleaved caspase + anti NeuN antibodoes) techniques. Future efforts will also be directed at using a combination of cleaved capsase staining with FluoroJade C staining as well as cleaved caspase counterstained with DAPI. FluoroJade C staining is a fluorescent staining technique that specifically stains injured neurons. Combining this Fluorojade C staining with cleaved caspase staining will help differentiate only injured cells (FJC) versus injured cells undergoing apoptosis (cleaved caspase +FJC).

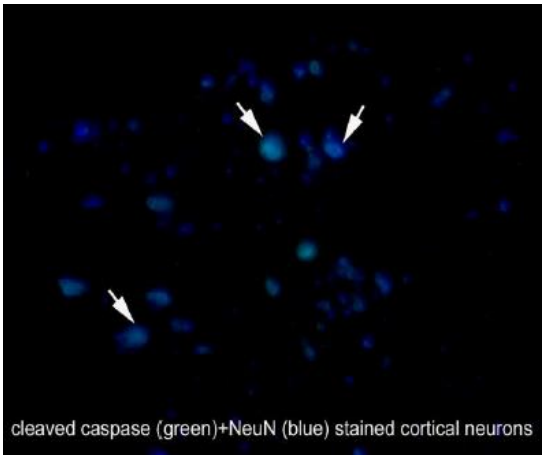

Figure 24 shows a representative area showing cortical neurons stained by dual labeling immunofluorescence (cleaved caspase-+NeuN).

Development of a staining technique to assess cell injury using Fluorojade C and cresyl violet

A preliminary staining of representative brain sections from 1 blast and 1 sham animal by Fluorojade C was performed. Fluorojade C is a sensitive fluorescent staining technique to visualize injured neurons. Free floating sections were immersed in 100% ethyl alcohol for 3 minutes followed by a 1 minute change in 70% alcohol and a 1 minute change in distilled water. The sections were then transferred to a solution of 0.06% potassium permanganate for 15 minutes and were gently shaken on a rotating platform. The sections were rinsed for 1 minute in distilled water and were then incubated in FluoroJade C solution (0.0001%) for 30 minutes. The sections were then rinsed with three 1 minute changes of distilled water, mounted on a slide and coverslipped with D.P.X. Figure 25 shows FluoroJade C labeled neurons, indicated by arrows. Current efforts are directed at optimizing this staining technique and implementing this method by using sections from all the blast (n=5) and sham animals (n=4). Furthermore, a preliminary cresyl violet staining was performed on representative sections (Figure 26). This staining technique will be used in conjunction with FJC and cleaved caspase to assess cellular injury.

Serum analysis for injury markers

During this period, we also performed a preliminary ELISA analysis of serum samples from 5 blast and 4 sham animals for the presence of injury markers, neurofilament-heavy chain and glial fibriallry acidic protein. These ELISA analyses were performed using the commercially available kits and we are in the process of analyzing this data.

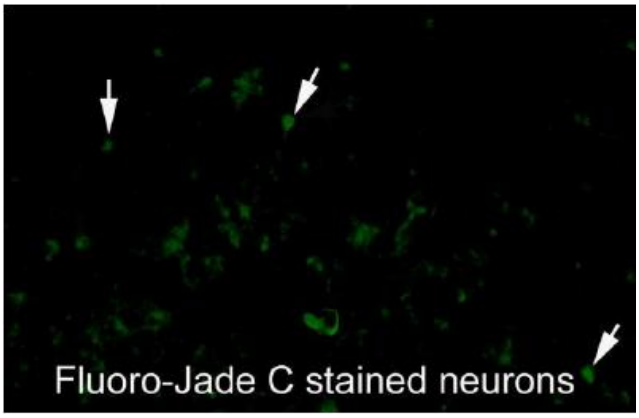

Figure 25 shows a representative area showing cortical neurons stained by FJC staining

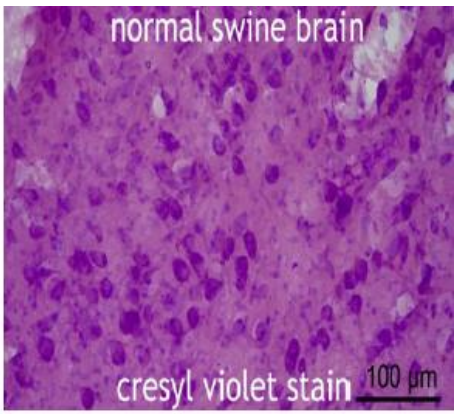

Figure 26 shows a cresyl violet stained representative area showing cortical neurons.

TASK II REPORT

Task II – Perform open field blast testing on 6 unembalmed post-mortem human subjects (PMHS) also known as cadavers to obtain biomechanical data

PMHS blast testing was initiated during this reporting period We were able to obtain one male specimen from Platinum Training, suitable for our use. It arrived in the lab about four days after death and it was tested on the ninth day. Also, during the post-mortem period prior to instrumentation, the specimen was kept at 4 C. Relevant biological data on the specimen are provided in Table 7.

Table 7. PMHS Data

PMHS ID	Sex	Age	Height	Weight	COD
BRC13102001	Male	72	66''	147 lb	Cardiovascular Disease

1. PMHS Preparation

Six intracranial Kulite pressure sensors were inserted into the frontal, parietal, left/right temporal, and occipital region of the skull. A detail description of sensor location is shown in Table 8 and Figure 27. An acceleration block containing three linear accelerometers and three angular rate sensors, and seven strain gages (frontal, parietal, right temporal, occipital, mandible, zygoma, and sphenoid) were fixed onto the skull surface (see Figure 27).

Table 8. Intracranial pressure sensor locations (X: A-P direction; Y: L-R direction)

Frontal	X: 50 mm anterior to Bregma Y: 20 mm away from mid-sagittal
Parietal	X: 20 mm posterior to Bregma Y: 20 mm from mid-sagittal
Temporal	X: 20 mm posterior to Bregma Y: 40 mm superior to ear channel
Occipital	X: 20 mm anterior to Lambda Y: 20 mm from mid-sagittal
All sensors were inserted to a depth of 5 mm below the cortex, except for the central brain which was at a depth of 50 mm below the cortex	

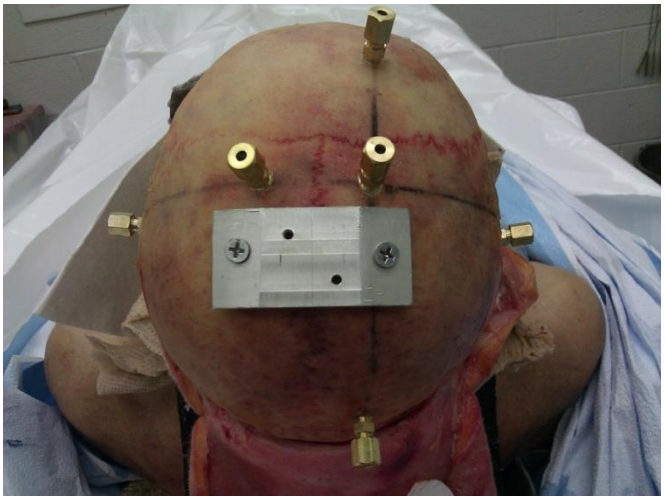

Figure 27. Location of ICP sensors and accelerometer block

2. Blast testing of PMHS

PMHS blast tests were conducted on 10/18/13 at ARES, Inc. in Port Clinton, OH. The explosive used was 8 lb of C4 placed at varying distances from the cadaver's head. The three pre-determined peak pressure levels were nominally 150, 300 and 400 kPa.
A total of 9 tests were conducted on the cadaver. The test subject was hung upside down at the knee on the A-frame (see Figure 28) so that it can be easily turned to accomplish frontal lateral and rear blasts. A T-frame was fixed to the cadaver back using a five-point harness system. Sand bags and straps were attached to the T-frame to limit the motion of the upper body of the cadaver. In addition to the measurement of intracranial pressure, strain, head linear acceleration, head angular velocity and head surface pressure were measured frontally and occipitally.

Figure 28. Photograph of the test site and set up for the cadaver test

3. Summary of Results

Intracranial pressure and accelerometer data were filtered at CFC 6000 and angular rate data were filtered at CFC 3000. All data from this cadaver have been processed. Sample plots are provided in this report. Figure 2.3 is a plot of ICP as a function of time for a low level frontal exposure. The symbols F, P, T, O and C stand for frontal, parietal, temporal, occipital and central sensors respectively.

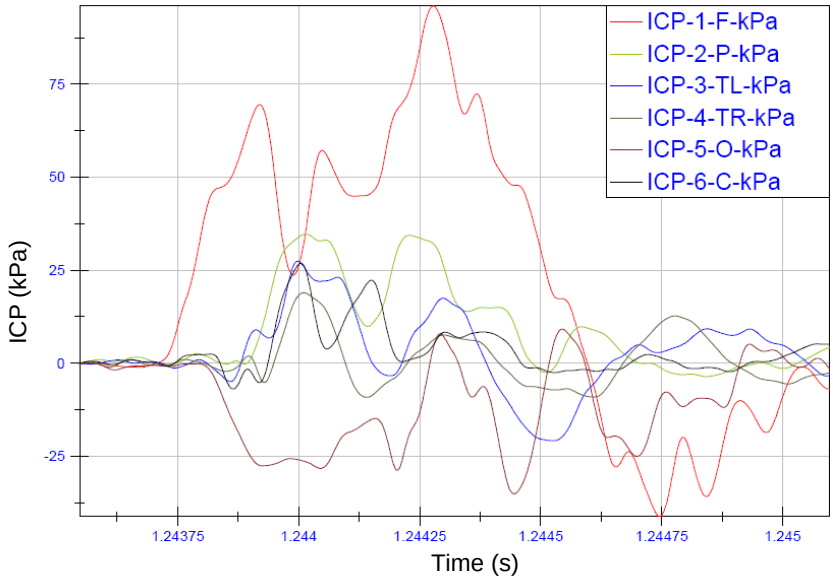

Figure 29. Intracranial pressures at various locations for a low level frontal blast. For a high level frontal blast, the intracranial pressures are shown in Figure 30.

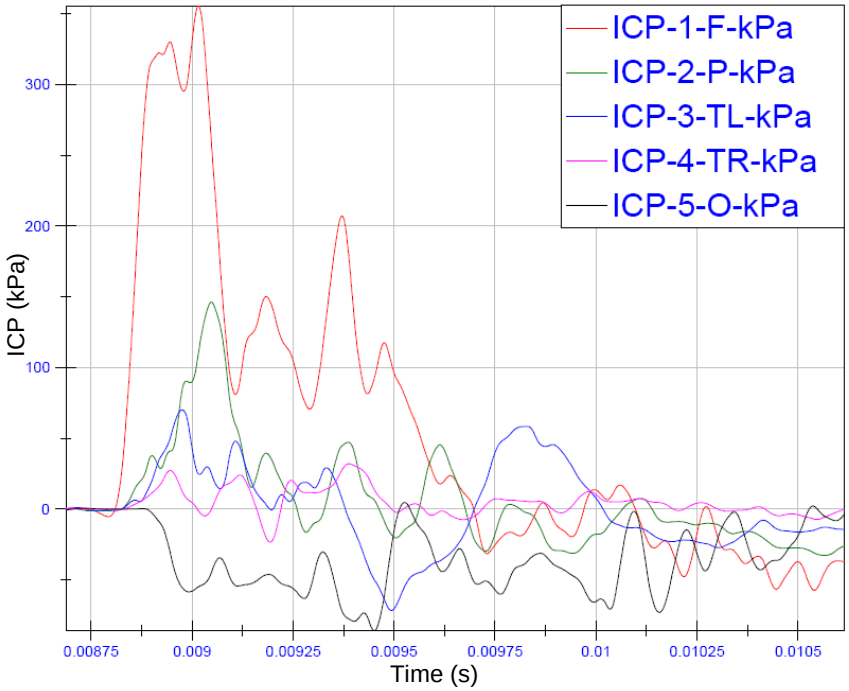

Figure 30. Intracranial pressures at various locations for a high level frontal blast

In both Figures 29 and 30, the measured intracranial pressures were lower than the IOP. The same holds for side blasts except that there is evidence of a contrecoup (negative) pressure, as shown in Figure 31

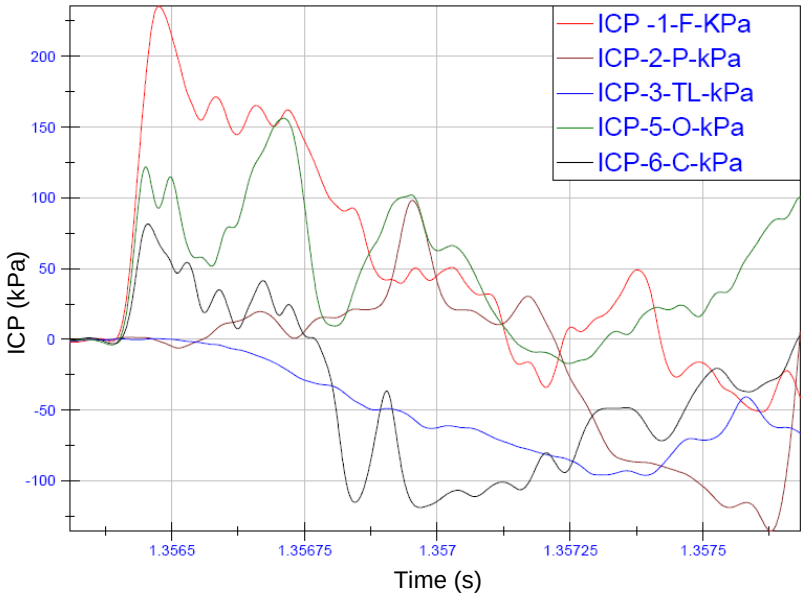

Figure 31. Intracranial pressures at various locations for a high level side blast

For rear blasts, there are multiple peaks in the intracranial pressure but there is also evidence of a contrecoup (negative) pressure, as shown in Figure 32.

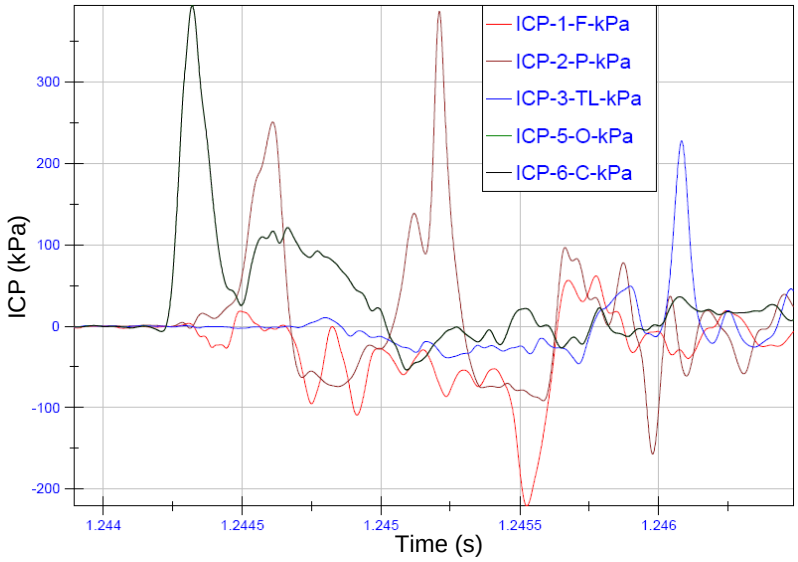

Figure 32. Intracranial pressures at various locations for a low level rear blast.

Head accelerations were very high but of short duration. In frontal and side blasts, the peak head accelerations were as high as ±1000 g and for rear blasts, the maximum A-P acceleration was 3000 g. The durations were all less than one millisecond. Measured head acceleration may be due to local bending effect from the accelerometer block and does not represent global head motion. At later post ignition, both translational and rotational motions of the head are minimal. The acceleration and angular velocity data are shown in Figures 33-35 for frontal, side and rear high level blasts, respectively.

The strain gage data were extremely variable and difficult to interpret. Analysis of these data has been postponed.

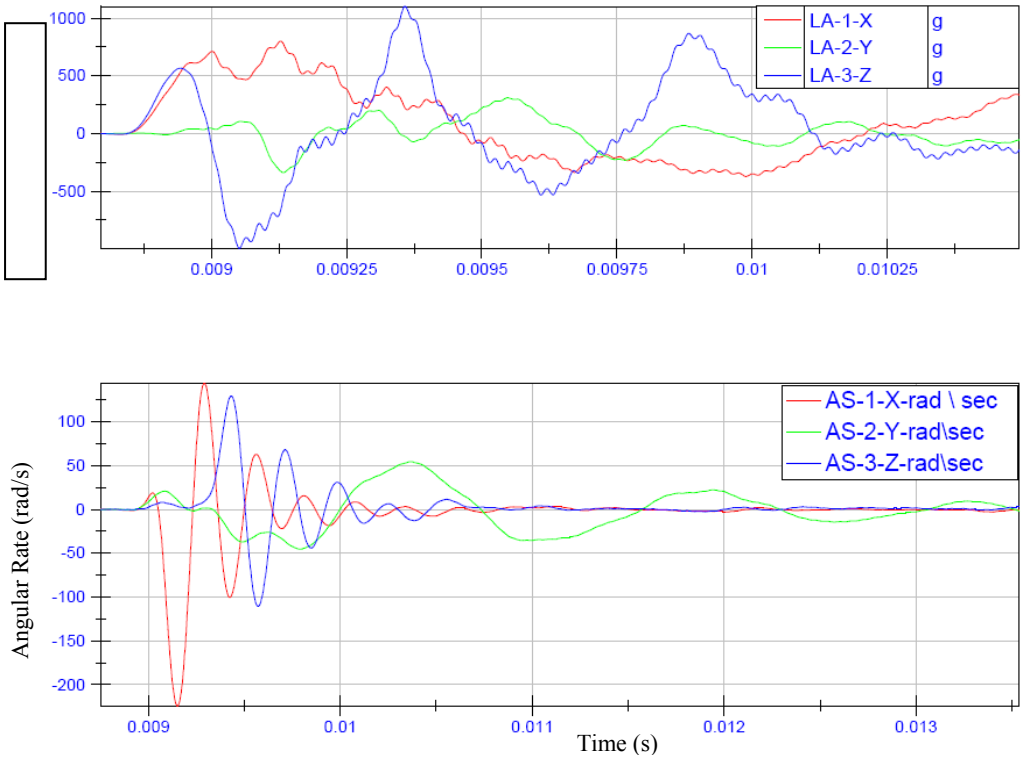

Figure 33. Linear acceleration and angular velocity for a frontal high level blast

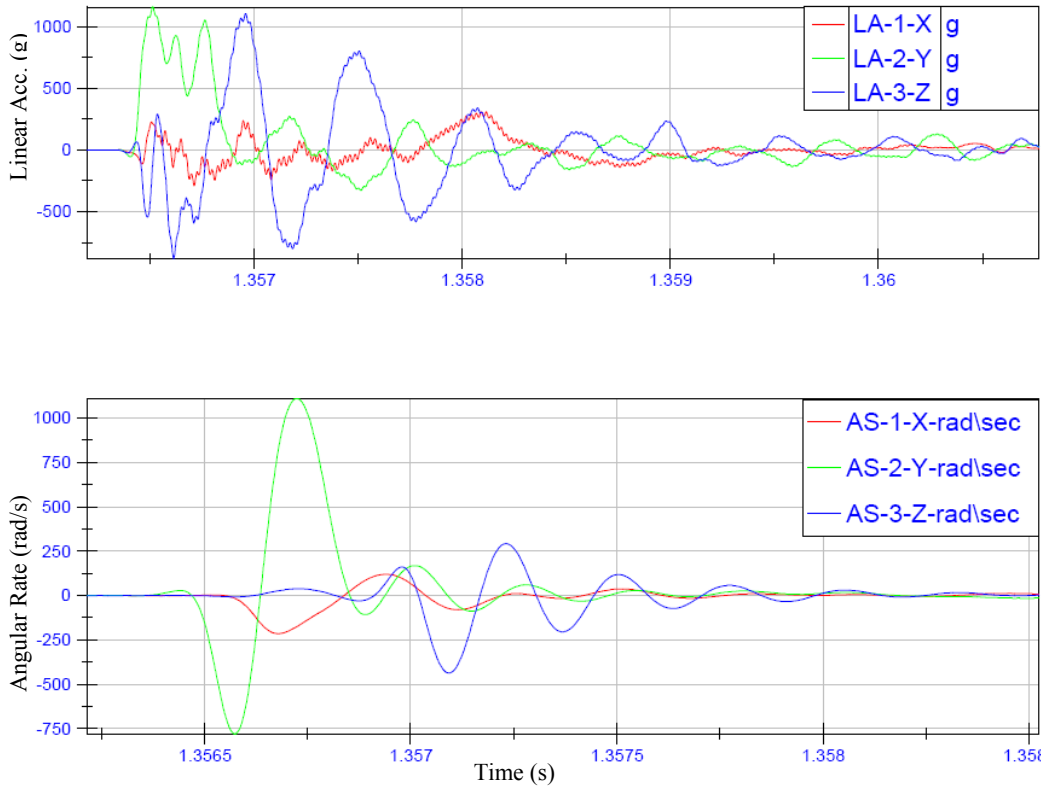

Figure 34. Linear acceleration and angular velocity for a high level side blast

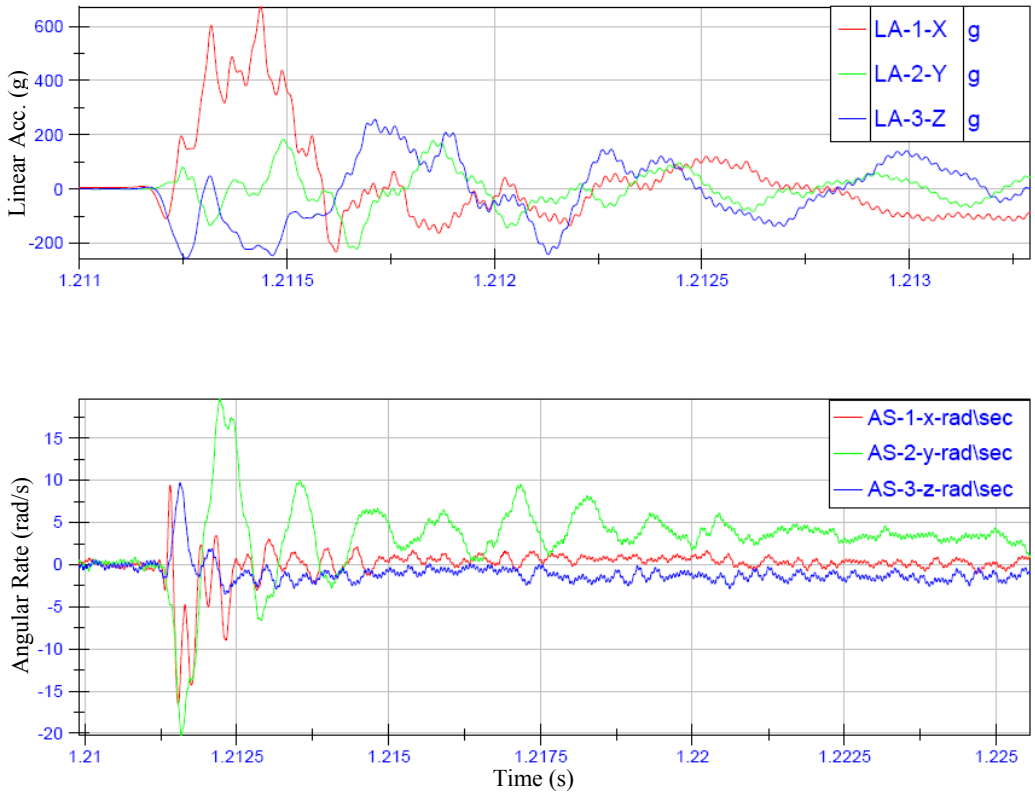

Figure 35. Linear acceleration and angular velocity for a high level rear blast

No conclusions can be reached with data from a single specimen. We will continue to analyze the data and collect more test data before we can arrive at some conclusions.

TASK III REPORT

Task III - Develop and validate a computer model of the pig brain simulating the effects of a blast over-pressure

In this reporting period, we worked on three aspects of pig head modeling:

1. Improvement of the 3-D finite element (FE) mesh of the pig head
2. Modeling air blast wave propagation using a 2-D to 3-D mapping technique
3. Simulations of the pig head response under blast loading.

1. Improvement of the 3-D FE Mesh of the Pig Head

The 3-D FE pig head mesh developed in the last reporting period was further refined to improve its bio-fidelity. The brain has been partitioned into different regions according to the anatomic atlas, as shown in Figure 36.

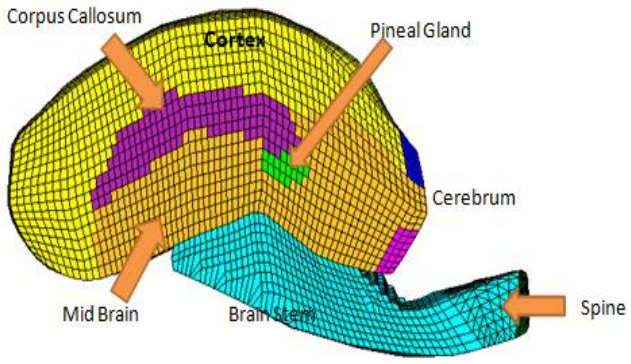

Figure 36. Partitions of the pig head model (cross-sectional view)

A careful examination of the pig head model revealed that some nodes at the boundary of brain and brain stem were not properly connected. Such node mismatches could result in inaccurate pressure transmission. A manual adjustment was performed to move the mismatched nodes to ensure that they are fully merged at the interface. The location with mismatch issues is marked with a red rectangle in Figure 37(a). The enlarged view of the mismatched nodes before and after the adjustment can be seen in Figures 37 (b) and (c), respectively.

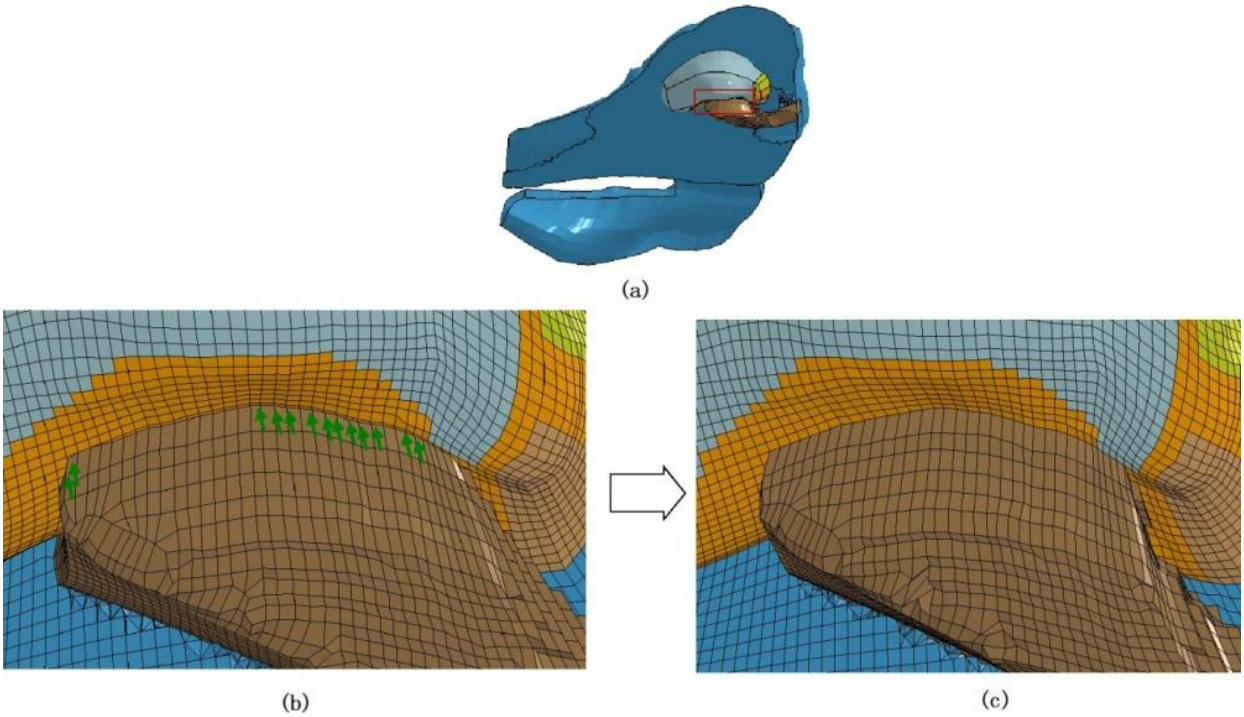

Figure 37. Node adjustment at the interface of the brain and brain stem: (a) The location with mismatch issue; (b) The mismatched nodes marked with green arrows; (c) The merged nodes after adjustment

The head model was then further improved to eliminate stress concentrations detected close to the sharp boundaries between brain and skull. In the earlier model, there were some disconnected elements near the ocular orbits and in the auditory cavities (as marked in Figure 38). This issue was resolved in the current version of the pig head model by manually adjusting the mesh at these locations. Further mesh adjustment will be made on the outside surface of skull to reduce the sharp curvature changes.

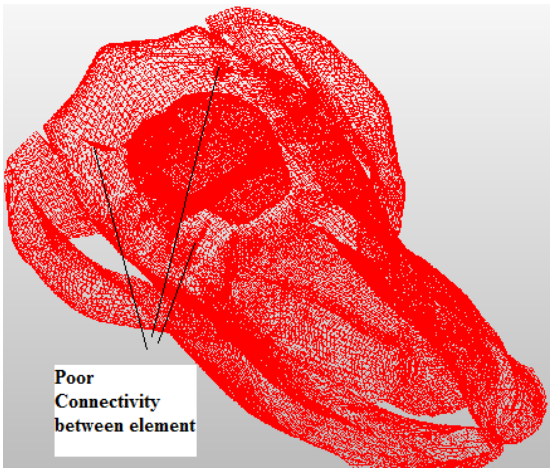

Figure 38. Locations with element disconnect issues

2. Modeling air blast wave propagation using a 2-D to 3-D mapping technique

In this section, numerical models were developed to simulate the propagation of the blast wave through air. The purpose is to reduce computation time. Our model includes the detonation of the explosive charge and the calculation of the IOP on the head requires transmission of the shock wave from the charge to the head through the atmosphere. Since the air domain requires a large number of elements, a 2-D to 3-D mapping technique was used to save computational time without loss of accuracy. This technique first simulates the shock wave propagation in a 2-D air domain before the shock front reaches the target (pig head). At the end of this phase, the results in the 2-D domain are mapped into 3-D air mesh and then the shock wave is coupled with the target in the 3-D domain. Since simulations with a 2-D mesh take less time than those in a 3-D mesh, the computational cost can be significantly reduced. The 2-D model setup for this study is shown in Figure 39.

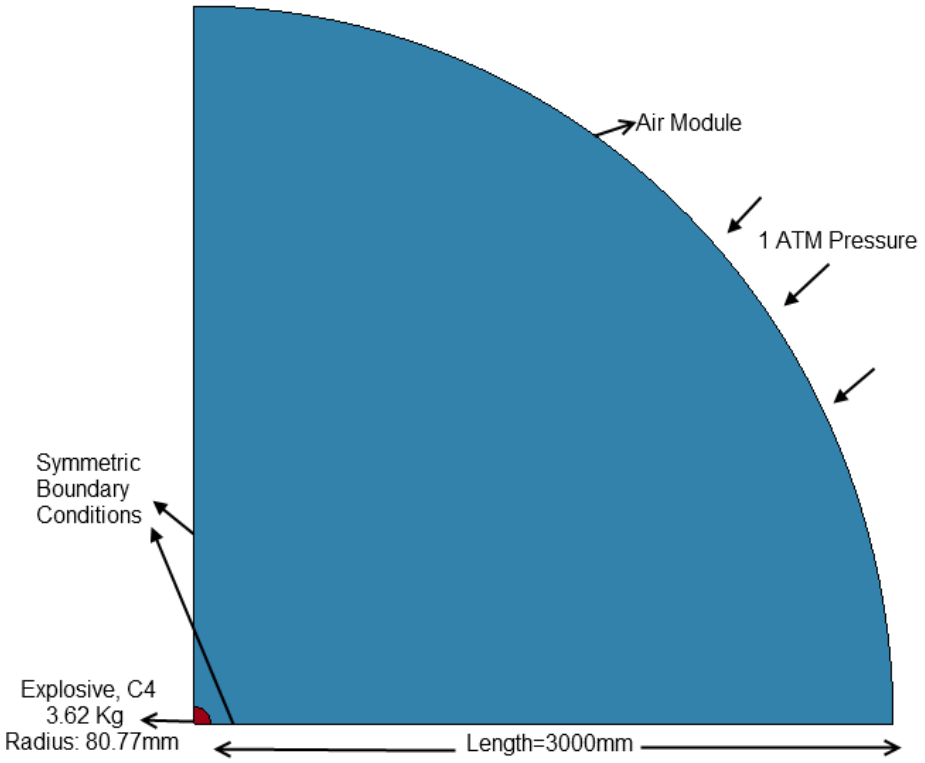

Figure 39. The model setup for a 2-D air domain and charge

In blast simulations, mesh size and mesh density of the air domain are key variables for matching the predicted thickness of the shock front and the magnitude of the pressure wave with those measured experimentally. A mesh sensitivity study was performed to determine the optimum size of the elements in the air domain. We compared our model results with the theoretical calculations using Conwep. Mesh sizes of 6.4, 4.8, 2.4, 1.2 and 0.9 mm were tried to see the effect of varying mesh density on pressure wave magnitude. Figure 40 shows the result of mesh sensitivity study. It was concluded that the solution converged for a 0.9-mm element size in the current case. The time history plot of blast overpressure is shown in Figure 41. The peak blast overpressure and its duration are in good agreement with the theoretically calculated blast incident pressure from Conwep. The pressure wave transmission in the air domain is shown as a sequence of blast events at different time steps in Figure 42. It is seen that an appropriate time to map the 2-D domain to the 3-D domain would be 1.5 ms after blast initiation. Figure 43 shows that pressure profile at the end of 1.5 ms has been successfully mapped to the -3D air domain at 1.5ms.

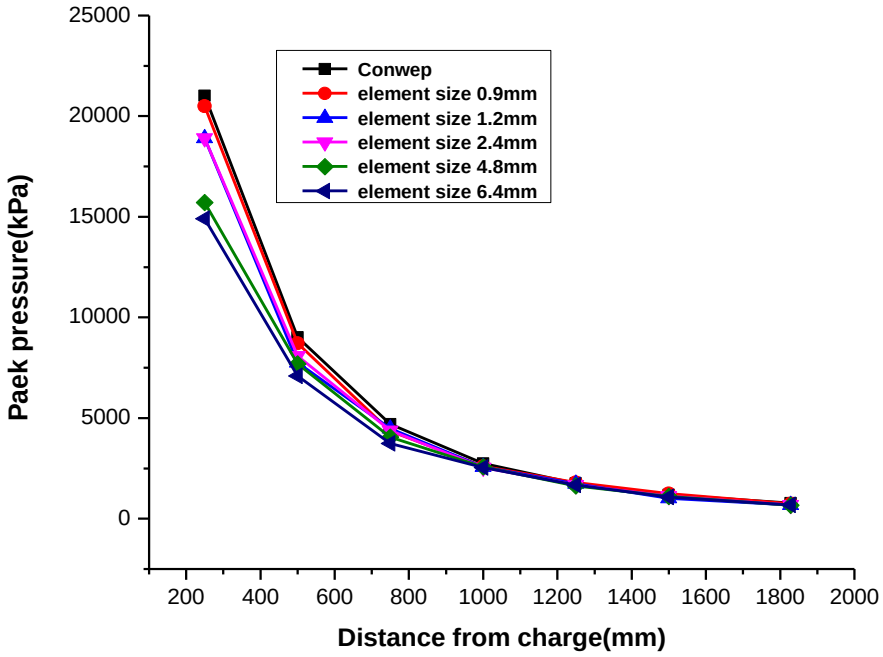

Figure 40. Comparison of the model predicted and theoretically calculated peak pressures for different mesh sizes

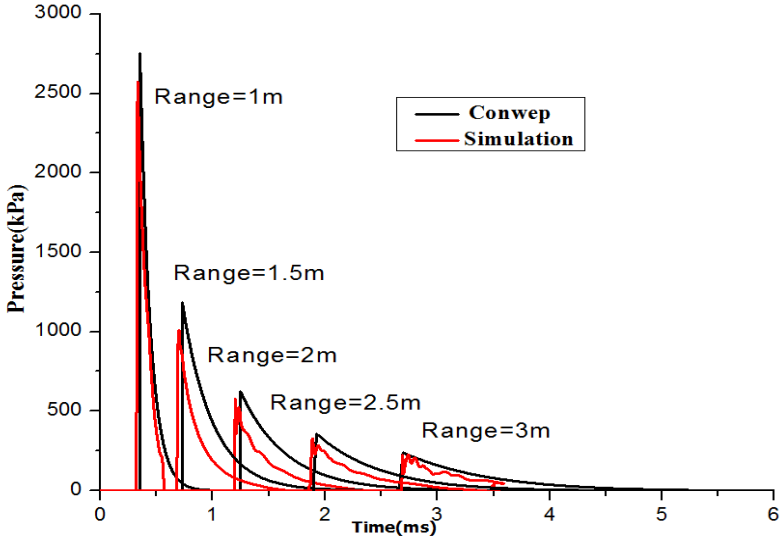

Figure 41. Comparison of the model predicted and theoretically calculated pressure waves

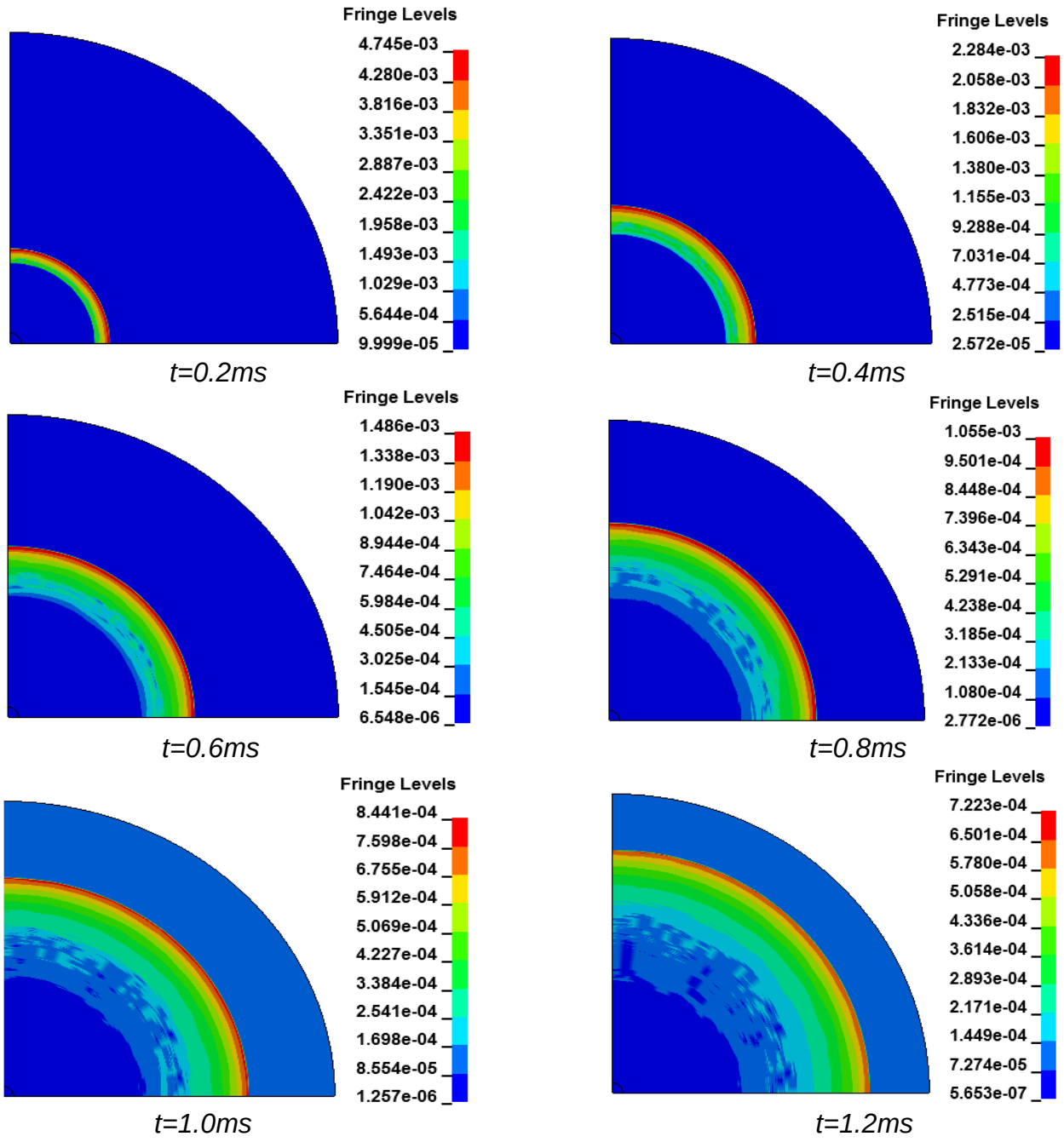

Figure 42. Pressure contour of the blast wave in the air domain at different time steps.

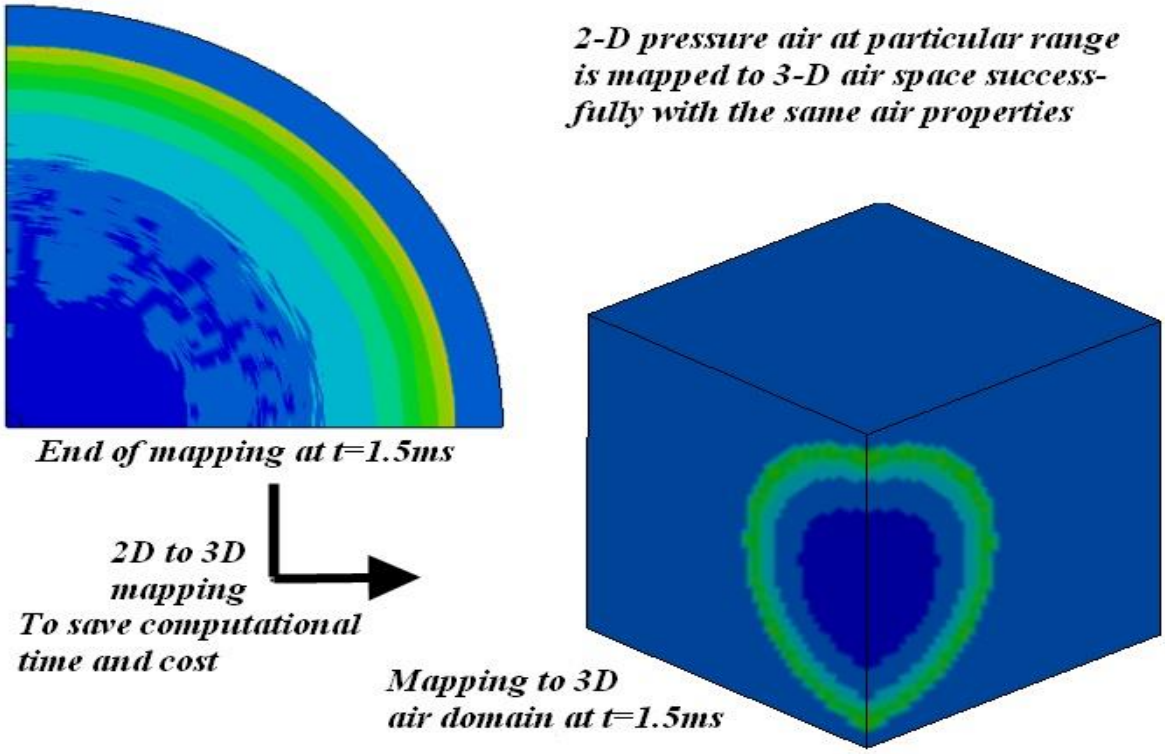

Figure 43. The procedure for 2-D to 3-D mapping

3. Simulations of the pig head response under blast loading

Once the pressure wave was successfully mapped to the 3-D air domain, a parametric study was conducted with the pig head model to examine the biomechanical responses inside the brain. Shock wave interaction with the target, i.e. the pig model in the 3-D domain used the fluid/solid coupling algorithm. The *CONSTRAINED_LAGRANGE_ IN_SOLID formulation available in LS-DYNA was used to model the coupling between the shock wave and the biomechanical surrogate.

Figure 44 illustrates the blast impact simulation setup with the pig head and brain model included.

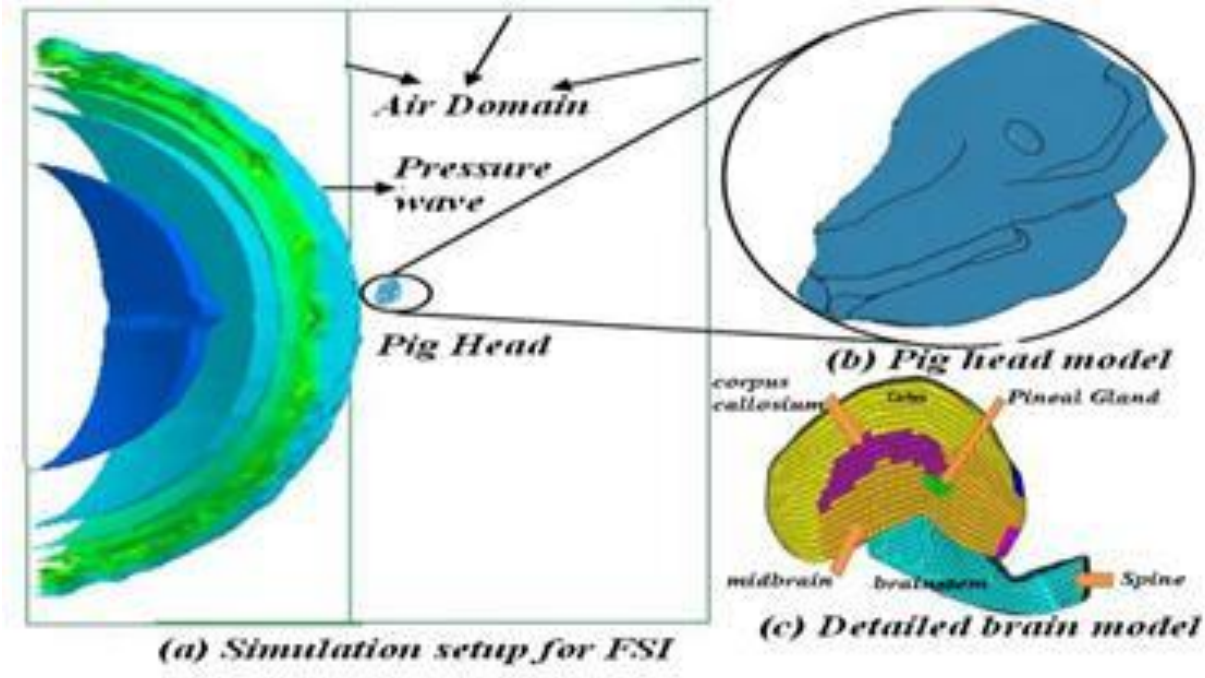

Figure 44. (a) Model setup, (b) Pig head model, (c) Detailed brain model

The biomechanical responses of the pig head in terms of regional distribution of intracranial pressure were compared with the preliminary experimental data at peak incident pressure level of around 300 kPa. The predicted intracranial pressures and the experimental pressure magnitudes inside the pig brain are shown in Table 9. The trends are similar to data available in the literature.

Table 9. Comparison of model predicted and measured incident pressure and intracranial pressure magnitudes

Sr No.	Air Pressure (kPa)	Intracranial pressures(kPa)					
	Incident Pressure	Frontal	Parietal	Left Temporal	Right Temporal	Occipital	Center
1. Experiment	324.2	336.0	638.4	442.1	561.4	377.3	291.3
2. Experiment	286.0	237.0	248.7	208.7	217.4	215.8	251.5
3. Simulation	298.0	410.0	344.0	319.0	338.0	286.0	326.0

Currently, due to limited experimental data sets and scatter in the available data, the simulations results for biomechanical responses are not in a good agreement with the

test results. More comparisons will be made once new experimental data become available.

Additional simulations were conducted on the aforementioned 3-D air blast model and pig head model. Special attention was paid to the boundary conditions of the pig head. In this section, three cases were considered: (1) both the skull and brain are intact; (2) the skull has a small opening while and the brain is intact; and (3) the brain has a small hole (air bubble) on the surface while the skull is intact. Case 2 is intended to study the effect of an unsealed hole on the skull during sensor installation in the physical tests; while Case 3 simulates the bubble between skull and brain. The sketches of Cases 2 and 3 are shown in Figure 45.

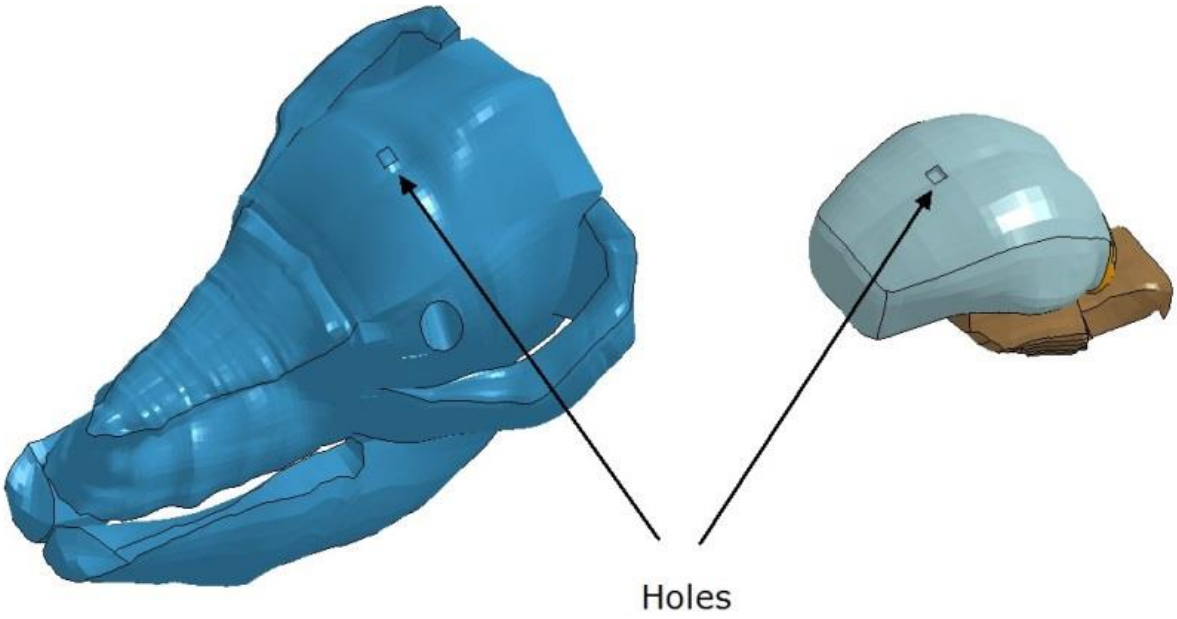

Figure 45. Simulation cases with openings in the skull and brain: (Left) The skull has a small opening while and the brain is intact. (Right) The brain has a small hole on the surface while the skull is intact.

The model predicted peak pressures in the central area of brain in all three cases are plotted in Figure 46. It can be seen that in Case 1, the peak ICP at the center of the brain is higher than peak incident pressure by about 25%. An opening on the skull slightly decreases the ICP, and a significantly pressure drop can be observed when a bubble exists on the surface of brain.

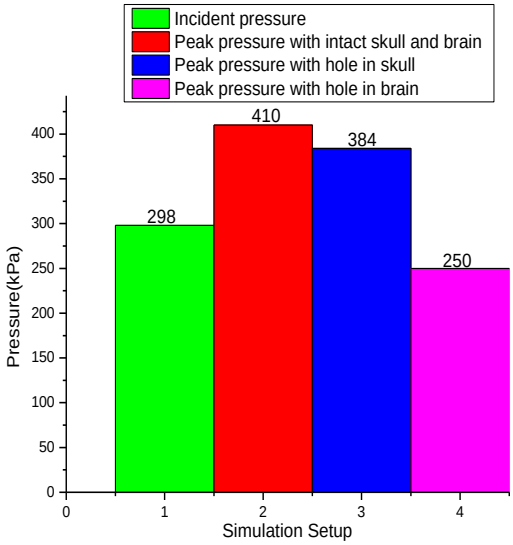

Figure 46. Comparison of model predicted ICP in three cases: 1) both the skull and brain are intact; (2) the skull has a small opening while and brain is intact; and (3)The brain has a small hole on the surface while the skull is intact.

A study of strain distribution in the brain was also conducted. Pig head response under blast wave loading was simulated for a duration as long as 30 ms so that head motion due to the blast wind can be included in the study the model predicted strains are shown in Figure 47. The results reveal that initial strains in the first 5 ms are low and that they are higher some time later. However, the magnitude is not high enough to cause injury if we use the criteria for strain related injury in blunt impact..The lower strain predicted by the model at the early stage is likely due to the primary blast pressure effect, while the subsequent higher strain is likely due to head motion. Maximum strains are found in the brain stem and occipital regions due to weaker constraints at these locations. It is therefore suggested that boundary conditions of the head model play an important role in strain distribution. It is necessary to further pursue to formulation more realistic boundary conditions for the brain model.

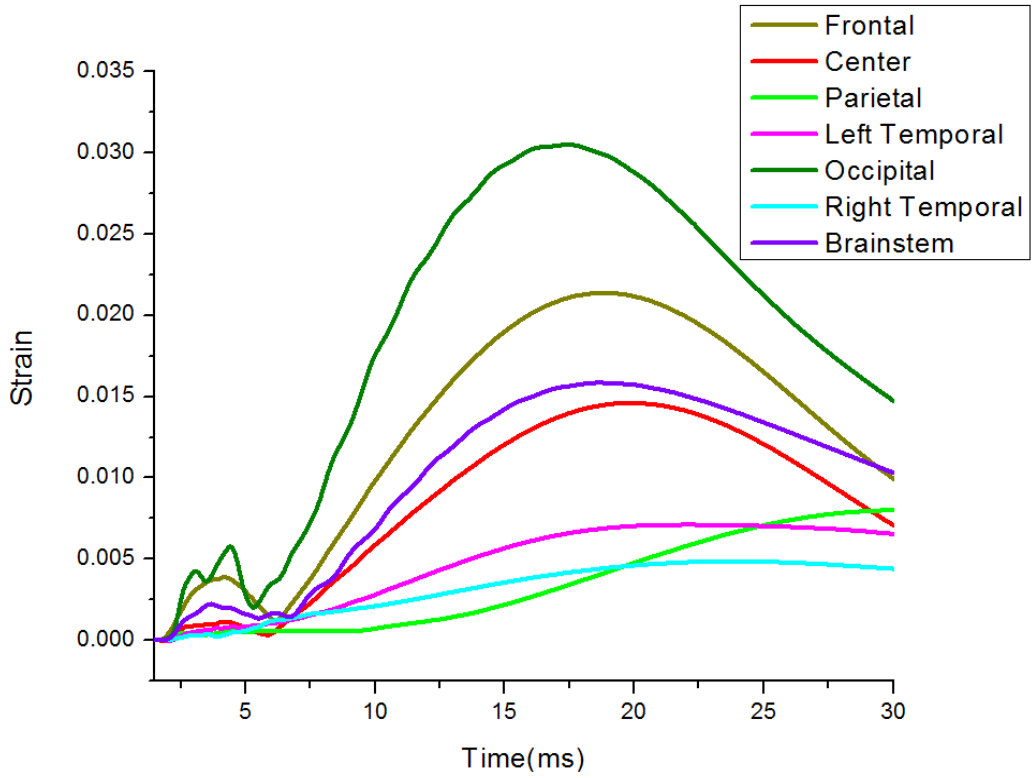

Figure 47: Strains predicted in the pig brain

TASK IV REPORT

Task IV - Develop and validate a computer model of the human brain simulating the effects of a blast over-pressure

In this task, we report work on three separate projects. 1) In preparation for blast testing of swine and cadavers, we set up the conditions to achieve three IOP levels by conducting preliminary tests in the absence of test subjects to make open field IOP measurements. Upon completion of the testing last year, we analyzed the IOP measurements to ensure that they are consistent and repeatable. 2) The human head model was exercised to compute brain strain due to blast overpressure and 3) an alternate boundary condition for the brain-skull junction was proposed and tested. Thus, the areas of study are:

1. Measurement and Analysis of Incident Overpressure (IOP) in Open Field Blast Test
2. Improvements to the Human Head Model
3. Computer model of the human brain simulating the effects of a blast overpressure

1. Measurement and Analysis of Incident Overpressure (IOP) in Open Field Blast Test

a) Open Field Blast Test Setup and IOP Measurements

Previously, in the 4th Quarterly Report, we used theoretical calculation along with FE analysis based on COMWEP, to determine the appropriate standoff distance, charge height and specimen height required for a test specimen (swine and cadaver) to be exposed to a single Friedlander blast wave with no interference from ground reflections. The desired peak overpressures of 150, 300 and 400 kPa peak overpressure were to be generated by an 8-lb sphere of C4 explosive charge. Prior to the actual test, the blast overpressure profile (peak and wave pattern) and its repeatability were measured and verified using three PCB pencil pressure probes (Model PCB 137A24, PCB Piezotronics, Inc., Depew, NY) during nine open-field blast validation tests conducted at the ARES, Inc. blast site in Port Clinton, OH.

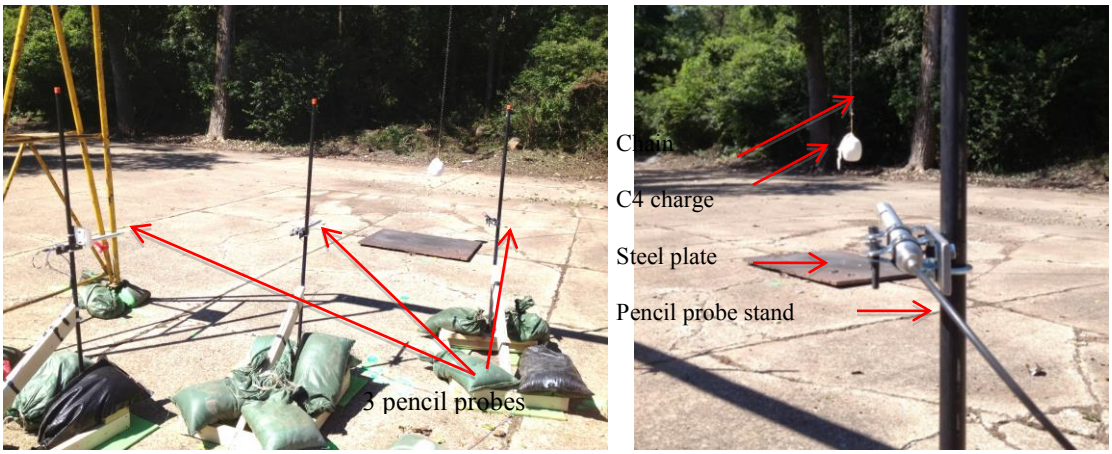

Figure 48: The photos showing the three pressure probes mounted on the frame at three locations with the axis of the pencil probe alinging with the center of the C4 charge suspended on a chain

1 million samples/second (sps) or Hz per channel. The digital data were post processed with a 100-kHz filter. Table 10 lists the final blast setup configuration for a total of 32 blast tests we have conducted so far on eight swine and one cadaver.

b) Analysis of Incident Overpressure (IOP)

A total of 32 8-lb C4 explosives were detonated during 6 testing days according to the parameters specified in Table 10. For some tests, after reviewing the actual pencil probe measurements at three standoff distances following the first test, the standoff distance for the next test might be adjusted to match the desired overpressure level. Figure 49 shows examples of pressure waves measured by the pencil probes. It is obvious that the pressure-time histories resemble typical Friedlander waveforms in a free field.

The peak overpressure values measured for all 32 tests are plotted in Figures 50 and Figurer 51 shows the average blast overpressure, average standoff distance along with standard deviation calculated within each blast level. Overall, the peak blast overpressure magnitudes were quite repeatable, particularly at the low blast level (150 kPa). The peak pressure magnitudes met the targeted low and high levels. The average medium pressure (280 kPa) was lower than the target level of 300 kPa. So far, a total of three instrumented swine, five non-instrumented swine and one cadaver have been exposed to 32 blasts. In addition, the temperature, wind speed, wind gust, wind chill, attitude and barometric pressure during each testing day were monitored by a pocket weather meter (Kestrel 2500).

Table 10: Open field blast test configuration for charge height, standoff distance and specimen height

Nominal incident overpressure level, kPa/psi	Standoff Distance, meter/inch	Specimen Height, meter/inch	Charge Height, meter/inch
150 / 21.8	4.72 / 186	0.91 / 36	0.66 / 26
300 /43.5	3.56 / 140	0.91 / 36	0.66 / 26
400 / 58	3.10 / 122	0.66 / 26	0.66 / 26

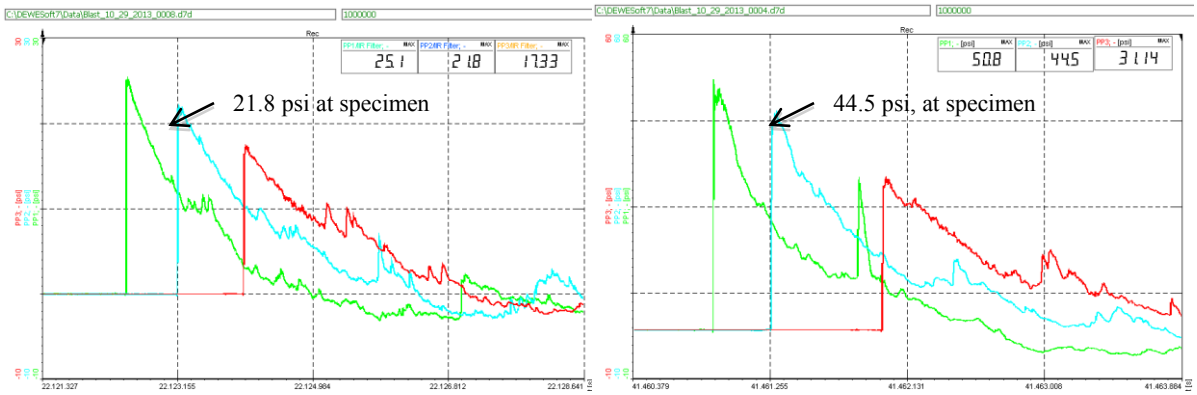

low medium

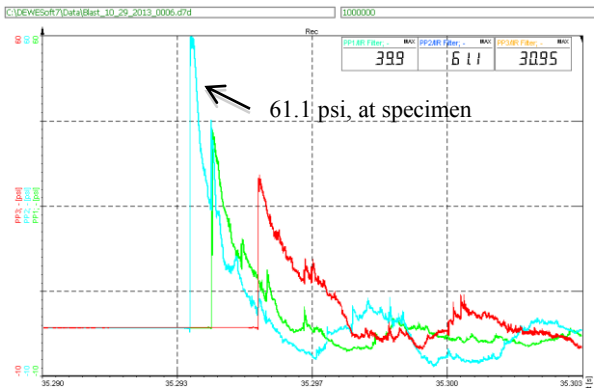

high

Figure 49: Examples of incident pressure wave in air recorded by pencil pressure probe at three desired blast levels.

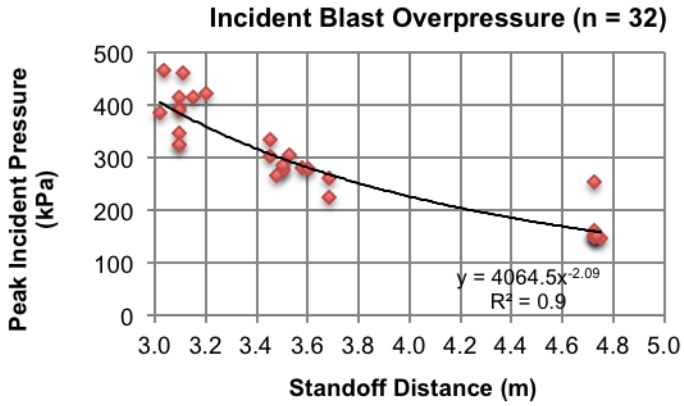

Figure 50: Peak blast overpressure measured at specimen location from a total of 32 blast tests.

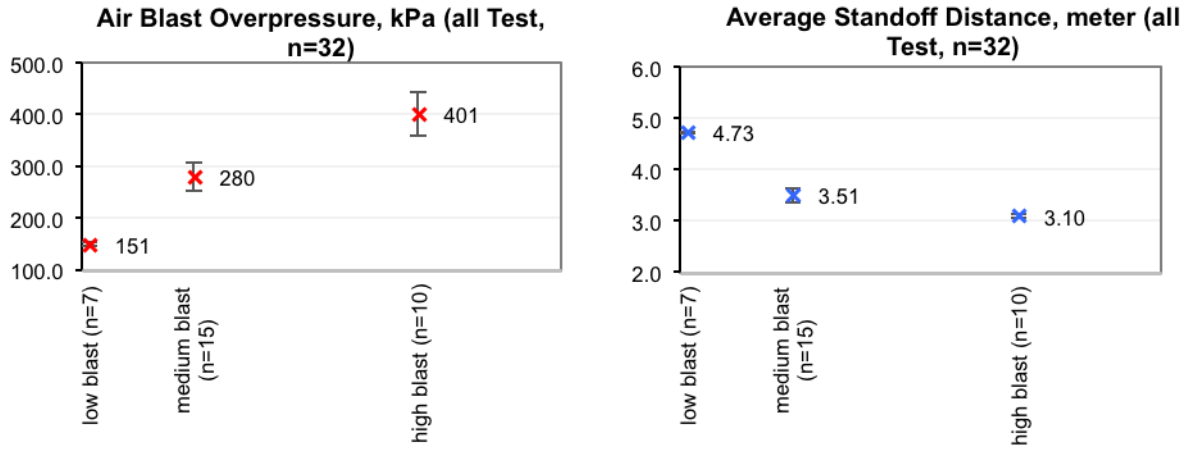

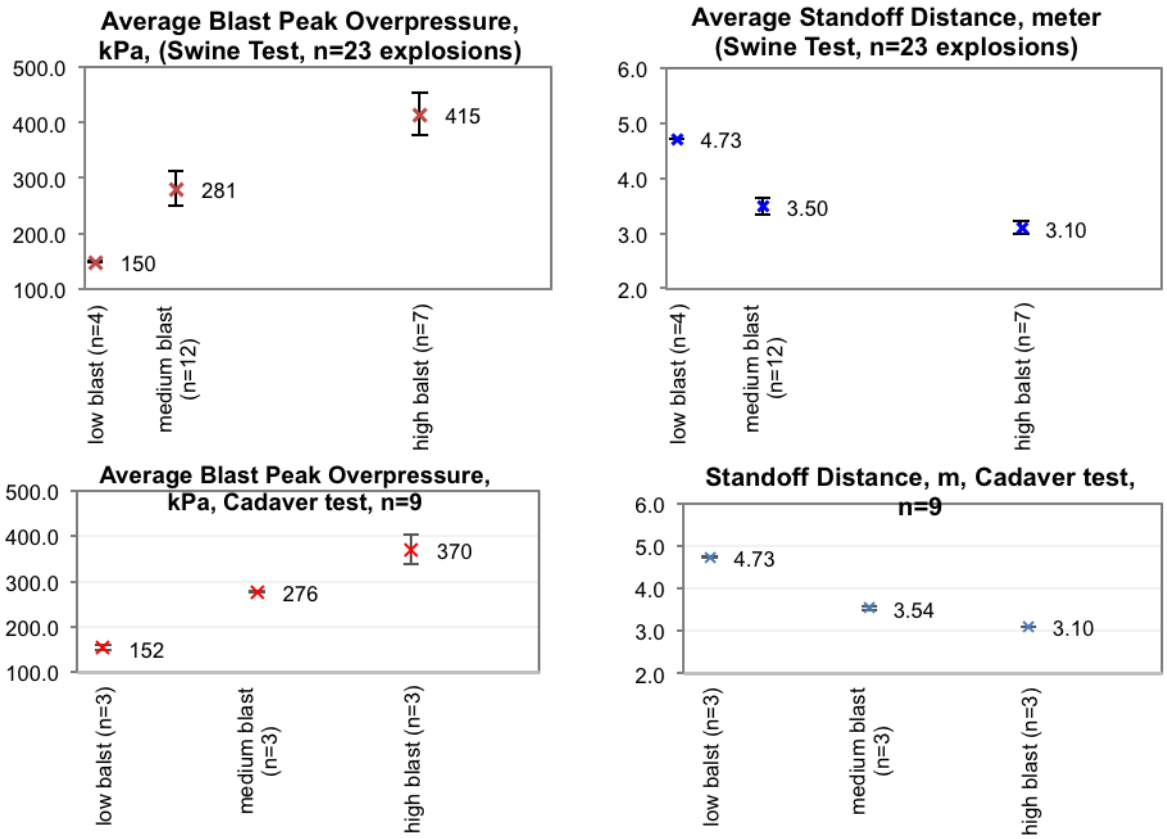

Figure 51. Calculated average peak overpressure and the corresponding average standoff distance measured at specimen locations for each blast level from all 32 tests - 23 swine tests, and 9 cadaver tests.

2. Improvements to the Human Head Model

The Wayne State University Head Injury Model (WSUHIM) is a finite element model that was developed previously with high resolution and many essential anatomical structures/regions of a human head and brain. The WSUHIM simulates the scalp, the skull with an outer table, diploë, and inner table, dura, falx cerebri, tentorium, pia, sagittal sinus, transverse sinus, cerebral spinal fluid (CSF), hemispheres of the cerebrum with distinct white and gray matter, cerebellum, brainstem, lateral ventricles, third ventricles and bridging veins. The facial model consists of facial bones, nasal cartilage, temporal mandibular joint, ligaments, soft tissue and skin. The entire head model is made up of over 330,000 elements and uses 15 different materials to simulate the various tissues of the head.

Previously we reported the development, validation and integration of the new human eye model to the current WSU head model in order to study the potential of injury to the retina and optic pathway induced by blast overpressure as well its association with neural and axonal injury occurring in other regions of the brain. In this reporting period, we completed the improvement to the brain model by refining some of the anatomical

structures and segregating additional detailed anatomical structures/regions into the current human head model so that heterogeneous, regional and anisotropic material properties can be incorporated into the model to better predict regional specific responses in blast-related TBI. Figure 52 shows the newly meshed brain structures

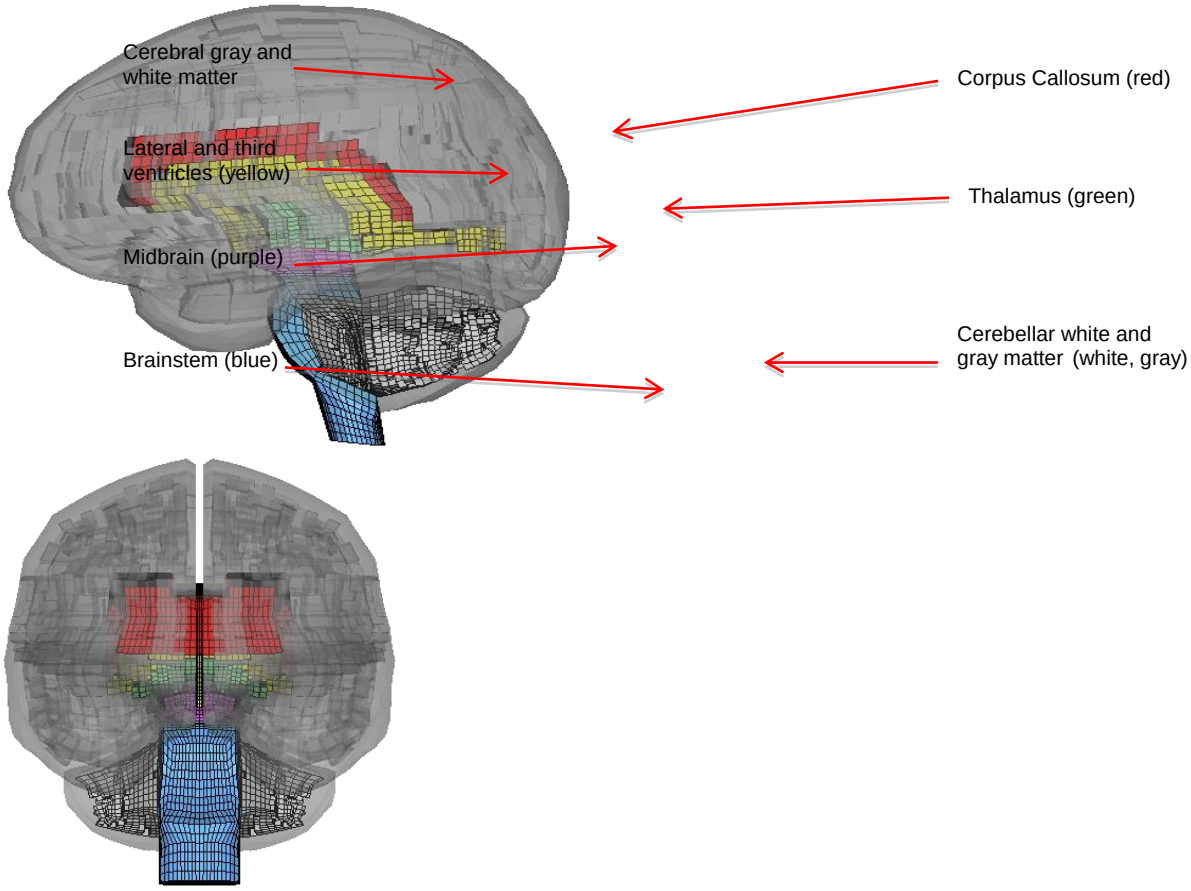

Figure 52: Lateral and anterior views of the improved WSU Head Model with cerebral gray and white matters displayed in transparent shade to depict the internal anatomical structures in the deep region of the brain

including the corpus callosum, thalamus, midbrain and differential white matter and the gray matter in the cerebellum. The size and volume of these anatomical structures conform to the data published in the literature.

3. Computer model of the human brain simulating the effects of a blast overpressure

The improved FE human head model was used to simulate PMHS blast tests described in Task II. The head model was positioned forward, sideways and backward with respect to the center of the charge according to the various stand-off distances. Three-dimensional FE models of 4.86 kg TNT (8lb C4 equivalent) and air were developed. The TNT and air material property definitions and their equations of state (EOS) were

the same as those utilized in a previous study by Zhang et al. (2013). The detonation and expansion of the explosive materials were described using the Jones-Wilkins-Lee (JWL) EOS along with a high explosive material property definition. The JWL equation (Eq. 1) is given by:

$$p = A\left(1-\frac{\omega}{R_1 V}\right)e^{-R_1 V} + B\left(1-\frac{\omega}{R_2 V}\right)e^{-R_2 V} + \frac{\omega E}{V}$$

Eq. 1

where *V is relative volume*. *E* is specific internal energy. *A, B, R_1, R_2, ω* are JWL fitting parameters. The parameters chosen were based on data in the literature (Dobratz and Crawford, 1985). The blast wave propagation in air, interaction with the head model and the subsequent structural response in the brain as the pressure wave was coupled with the various anatomical structures were simulated using the coupled multi-material Lagrangian-Eulerian, fluid-structural interface (FSI) and Lagrangian methods in LS-DYNA® 971 (LSTC, Livermore, CA).

The strain responses of the various anatomical structures were calculated throughout a 20 ms following the detonation. Figure 53 shows the temporal changes of brain strain in the white matter, grey matter, midbrain and brainstem regions due to a medium level frontal blast. In general, the brain strain peaked at 3-4 ms later after the ICP and linear acceleration reached their peaks, suggesting that the response of the brain tissue under blast loading is viscoelastic. The brainstem experienced the highest strain followed by the midbrain region (Figure 54). Whether this high strain is due to the foramen magnum boundary condition is under investigation. As of now only a single specimen has been tested. We plan to validate the model against experimentally measured pressure data in the cadaver head from the remaining 5 open field blast tests.

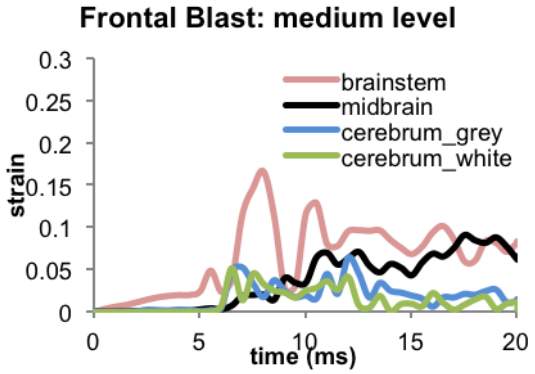

Figure 53. Brian strain temporal profile

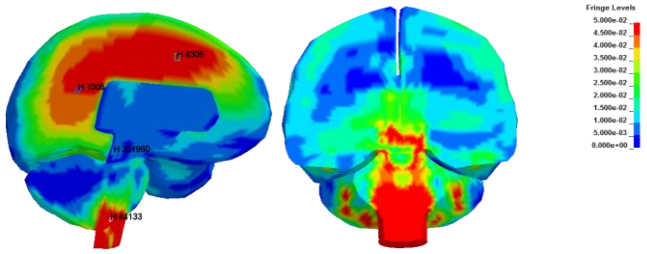

Figure 54,: Brain strain spatial profile in the mid sagittal plane and coronal plane through the thalamus

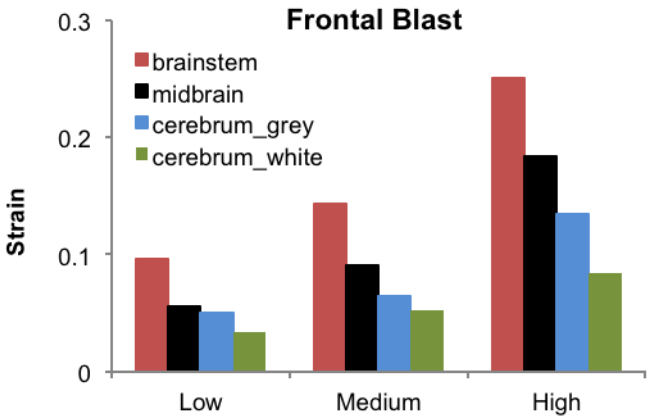

Figure 55. Comparison of the brain strain at various regions in response to low to high levels in the case of frontal blast

4. Examination of Boundary Conditions at the Brain/Skull Junction

In the current WSU finite element human head model, various anatomical structures and substructures of the brain and cerebral spinal fluid (CSF) were meshed and defined with Lagrangian formulation-based elements. The CSF fills the subarachnoid space between the arachnoid layer and the pia mater. Histological and morphological study showed that a variety of fibroblast-like trabeculae extend from the arachnoid to the pia mater. The trabeculae were found to be quite strong (Jin et al, 2007, 2011) and tether the brain to the dura. From anatomical and structural points of view, the CSF and the arachnoid trabeculae help suspend the brain within the skull. Considering the effect of fibrous trabaculae and the fluid nature of the CSF, the CSF was defined as a solid Lagrangian element with the bulk modulus of water (2.19 GPa) and a very low shear modulus (100 Pa). This modeling approach enabled the model prediction to match the brain skull relative motion data measured experimentally. Alternately, the Arbitrary Lagrangian Eulerian (ALE) elements with the Fluid Structure Interaction (FSI) can be used to model the CSF and the model results between the Lagrangian CSF and ALE CSF were compared.

To simply the model effort, a head model with an idealized geometry was developed. The head model consisted of the scalp, skull, CSF and brain structures (Figure 56). The head model was subjected to blast incident overpressure of 150 kPa. The ALE CSF was currently defined as water along with a Mie-Gruneisen Equation of State (EOS) in LS-Dyna 970 (Equation 1) (Liu et al., 2003). Note that trabeculae were not included in the ALE algorithm since the CSF was defined as a liquid. The pressure behavior of water in compression was defined by Equation 2 (Liu et al., 2003). Figure 12 shows the resulting intracranial pressure at brain location 1 (frontal region) and location 2 (lateral or parietal region). The pressure patterns at the two locations were similar between the Lagrangian CSF and ALE CSF models. The peak positive and negative pressures predicted by the model with ALE CSF were generally less than 15% lower than those predicted by the Lagrangian CSF model. An appropriate EOS is needed to represent

the CSF material other than the water. Further validation is needed to determine the modeling approach for representing CSF behavior during blast event using the data measured from on-going cadaveric blast tests.

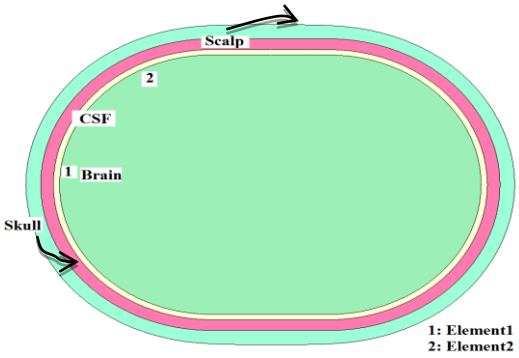

Figure 56: A simplified head model

$$\frac{U_s - C_0}{U_s} = S_1\left(\frac{U_s}{U_p}\right) + S_2\left(\frac{U_s}{U_p}\right)^2 + S_3\left(\frac{U_s}{U_p}\right)^3 \qquad \text{Eq. 2}$$

$$p = \frac{\rho_0 C^2 \mu\left[1 + \left(1 - \frac{\gamma_0}{2}\right)\mu - \frac{a}{2}\mu^2\right]}{\left[1 - (S_1 - 1)\mu - S_2\frac{\mu^2}{\mu+1} - S_3\frac{\mu^3}{(\mu+1)^2}\right]^2} + (\gamma_0 + a\mu)E \qquad \text{Eq. 3}$$

where U_s is shock wave velocity, U_p is fluid particle velocity, C_o is initial speed of sound, S_1-S_3 are the fitting coefficients, ρ_0 is initial density, C is the speed of sound, a is volume correction coefficient, γ_o is Gruneisen coefficient, and μ is ratio of the water density after and before disturbance.

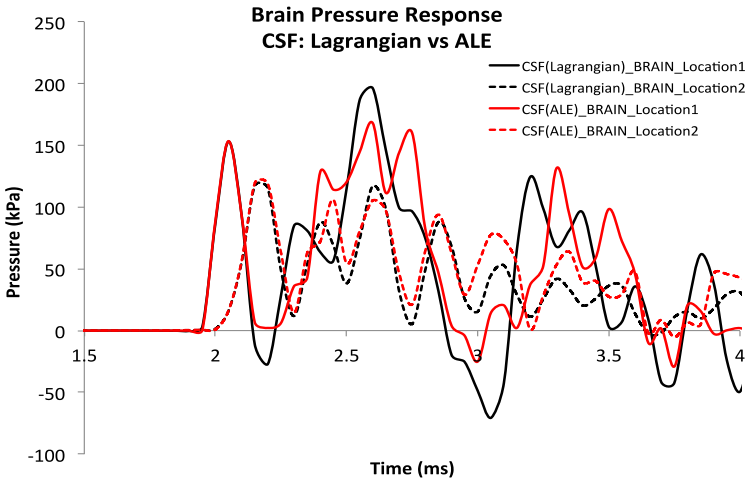

Figure 57: Comparison of the intracranial pressures predicted by the models where the CSF is modeled with Lagrangian or ALE elements

ADDITIONAL STUDIES

During the late fall of 2013 and the winter of 2014 when blast testing was suspended we did some additional studies on the pressure sensors used in our blast testing, in addition to the data analysis that was reported above. Also, the test site and test equipment were improved and a change in sensor array in the pig brain was proposed to streamline the swine testing procedure. The following accomplishments are reported:

1. Calibration of intracranial pressure sensors (ICP's) using a shock tube
2. Testing of ICP sensitivity to orientation with respect to the direction of blast
3. Improvements to the test site and test equipment
4. Change in sensor array to streamline instrumented subject testing procedure

1. Calibration of ICP Sensors

The plan was to calibrate all of our ICP's against a newly calibrated pencil (PCB) transducer used by Team Wendy to measure free field blast overpressure. Of ~~the six~~ all the Kulite pressure sensors that had been used for swine and cadaver testing last year, five were functional and these sensors were calibrated simultaneously inside a 12-inch shock tube located at the Bioengineering Center of Wayne State University. The calibration consisted of comparing side-on pressures. The Kulite sensors were bundled into a tight bundle and mounted to a block, as shown in Figure 1A. The white tips of the Kulite transducers are visible. The block was placed inside the shock tube with the pencil transducer right under the block so that all sensors would measure side-on pressure at the same location inside the shock tube. This is shown in Figure 1B in which the tips of the Kulites were pointing away from the camera and the pencil transducer is directly underneath the block carrying the Kulites.

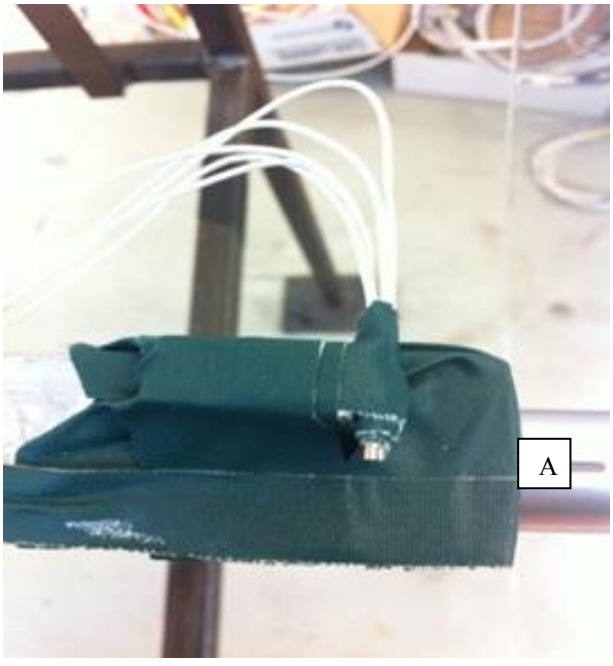

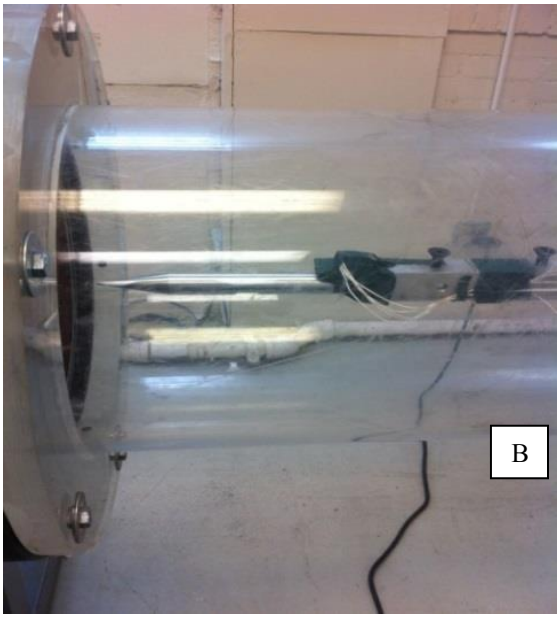

Figure 58. Experiment fixture in sensor calibration test. **A** shows the 5 ICP sensors bundled and attached to a block to measure side-on pressure inside a shock tube. **B** shows the location of the block inside the shock tube during the test.

The calibration results are shown in Figure 59 for all five sensors. The sensors were exposed to three almost identical blasts, using a driver pressure of 41.0 psi. The measured peaks values are shown in Table 11. An error analysis was performed to determine the accuracy of each sensor, using the pencil transducer as the standard. The average error was between -6 and +3% with no individual error greater than 10% (Table 12).

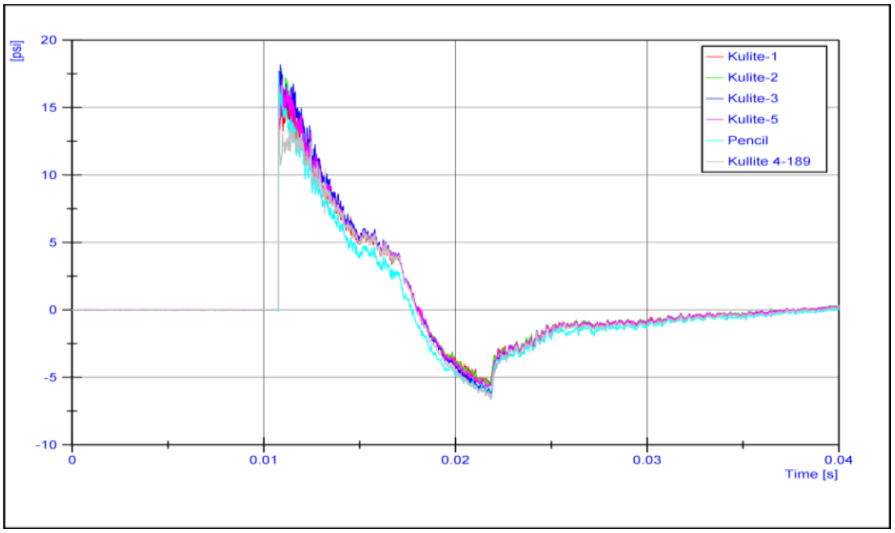

Figure 59. Test results from one of the three calibration tests

For the 2014 testing program, additional sensors will be pre-calibrated and used in the event the ones we are using now breakdown or are damaged.

Table 11. Kulite Pressure Sensor Calibration Data

Kulite and pencil calibration results in air (psi)								
Test ID	Mylar	Driver	Pencil	Sensor 1	Sensor 2	Sensor 3	Sensor 4	Sensor 5
2014-1-1	5+5	41.20	17.55	16.41	17.91	18.18	16.45	17.72
2014-1-2	5+5	41.05	17.27	16.71	17.55	17.90	15.70	17.72
2014-1-3	5+5	41.05	16.98	16.58	17.42	17.33	16.63	17.36

Table 12. Errors in Peak Pressure Compared to Data from Pencil Transducer

	Sensor 1	Sensor 2	Sensor 3	Sensor 4	Sensor 5
Test 1	-6.50	2.05	3.59	-6.27	0.97
Test 2	-3.24	1.62	3.65	-9.09	2.61
Test 3	-2.36	2.59	2.06	-2.06	2.24
Average	-4.03	2.09	3.10	-5.81	1.94

2. Testing of ICP sensitivity to orientation with respect to the direction of blast

There has always been a concern regarding the effect of orientation of the pressure sensors in the brain with respect the direction of blast. This concern arose from the fact we expose the animal to blast from three orthogonal directions using sensors that were pre-implanted in the brain and could not be re-oriented when the head was turned. That is, we wanted to know if there was a difference in the face-on and side-on pressure in the brain. Cadaveric human and swine brain were used in this experiment. For both the human and swine brain, the sensor was inserted into the frontal lobe of the brain and pressure measurements were made to record both the face-on and side-on pressure by rotating the head 90 deg in the shock tube.

For the swine brain, there was very little difference between face-on and side-on pressure, as shown in Figure 60. This result agrees with the principle in fluid mechanics which states that face-on pressures can be higher than side-on pressures if there is flow velocity component acting on the diaphragm of the sensor. It this case, the brain motion is negligible and therefore the two pressures should be the same. It should be noted that the measured peaks were both higher than the incident pressure.

Data from the sensor in the cadaver brain revealed that the face-on pressure was considerably higher than the side-on pressure and that the waveform of the face-on pressure was completely different from that of the side-on pressure and from the swine pressure data (See Figure 61). We believe that this is an artifact due to the presence of air/gases in the vicinity of the sensor. Also, the side-on pressure was found to be lower than the ambient pressure. We will try again with another cadaver head when it becomes available.

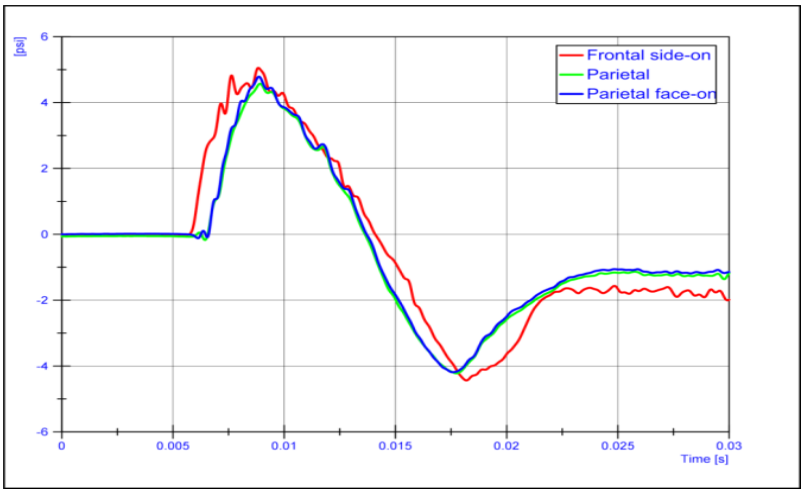

Figure 60. Comparison of face-on and side-on intracranial pressure in a swine brain

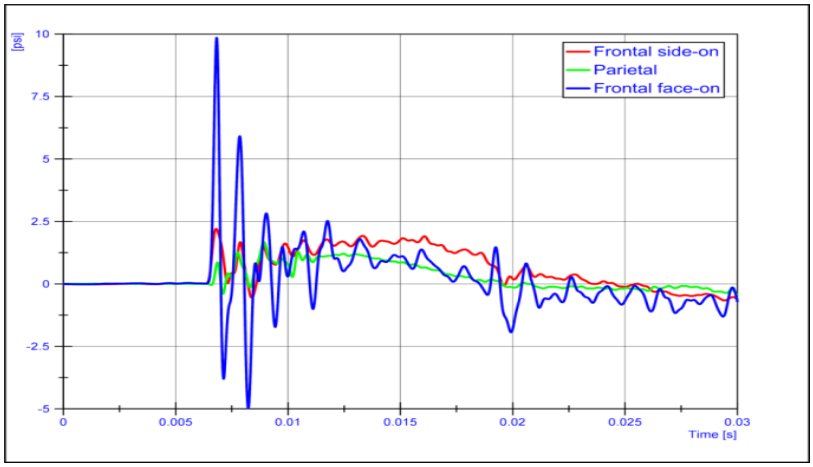

Figure 61. Comparison of face-on and side-on intracranial pressure in a cadaver brain

3. Improvements to the test site and test equipment

We have made several improvements to the open field blast site and to the test setup at ARES. Inc., in Port Clinton, OH, in collaboration with ARES, Inc. and with Team Wendy, who are tasked to measure the open air blast overpressure near the test subjects. The purpose of the modifications is to ensure the consistency of the blast wave profile to which the test subject is exposed and to maintain the accuracy of the blast overpressure profile measurements between tests. More specifically, the following improvements made were: 1) The base of the 12-ft steel A-frame gantry used to support the test subjects was rigidly anchored to the concrete ground. Last year, a number of sand bags were used to prevent the A-frame from moving due to the blast wind. 2) A large 3 m x 3 m, 1-inch thick steel plate along with a 1-inch thick rubber mat were acquired. They will be placed on the ground just below the C4 charge to replace a smaller plate used previously. This will help control the consistency of the ground reflections of the blast wave and reduce the amount of debris kicked up by the blast wave. 3) The wooden stands used for securing the PCB pencil probes were frequently damaged by the shock wave. Team Wendy has come up with a new design using a steel frame which is sturdier and can provide a more stable support for the pencil probe than the wooden frame. It will also be less prone to shock- induced damage.

4. Change in sensor array to streamline instrumented swine testing procedure

The original test plan was to instrument the brain of each swine with six miniature intracranial pressure (ICP) sensors and to expose the swine to 9 blasts (three forward, three lateral and three backward) on a single test date. Due to the extensive surgery and repeated blasts on the swine head, the survival rate of the anesthetized instrumented animals was very low. Among the 19 blast tests performed on instrumented pigs, only the first two tests were performed on live pigs; the remaining tests were performed after the pigs had expired. Also, time was very limited to prepare and perform 9 tests in one day. Thus, a revised sensor array for the remainder of the instrumented swine testing will be used. In this new instrumentation plan, we will use four ICP sensors in each swine. Instead of exposing each pig to blasts in all three directions, we will only test in the front/rear or side direction. This method will result in less damage to the swine brain from pressure transducer placement, will increase survival rate and allow for higher probability of completion of the proposed set of blasts in one day. By reducing the number of ICP sensors we will have more available channels in the data acquisition system, thus allowing us the option to perform tests on two instrumented swine simultaneously on the same test date. A detailed plan was drawn up and submitted to the COR for approval.

DISCUSSION

There is an apparent conflict in the results of the two models. The predicted strains for the swine are much lower than those for the human, as can be seen from comparing Figures 47 and 53 . Aside from geometrical differences in anatomy, the other major difference is skull thickness. Swine skull thickness is several times larger than that of the human and this difference may have a large effect on brain strain. We will continue to investigate this as it may show that the swine is not the best surrogate for the human for primary blast.

CONCLUSIONS

1. The swine testing program is well underway, having overcome many initial challenges of animal handling, test equipment set-up and histological techniques. It is on schedule and should be completed in 2014, leaving plenty of time for data analysis and histological studies
2. The PMHS program is also underway. We have also overcome many of the initial challenges listed in Conclusion #1 above. We were only able to obtain one specimen last year but hope to find and test the remaining specimens this year.
3. The swine brain model is well developed and is ready to be validated when more swine data are collected. Current ICP data are somewhat variable due to the fact that we cannot completely ensure that there is no air in the skull after the insertion of the ICP sensors and sealing of the skull.
4. The anatomical representation of the head model has been further refined. The head model is ready to be validated when more PHMS data are collected.

PUBLICATIONS AND PRESENTATIONS

Journal paper

Zhu F, Chou CC, Yang KH and King AI. A theoretical analysis of stress wave propagation in the head under primary blast loading. Proceedings of the Institution of Mechanical Engineers, Part H, Journal of Engineering in Medicine, 2014, Vol. 228(5) 439–445.

Conference papers

Kalra A, Zhu F, Yang KH, King AI. Key parameters in the blast modeling using 2D to 3D ALE mapping technique. In: Proceedings of 13th International LS-DYNA Users Conference, June 2014, Detroit, MI, USA.

Kalra A, Zhu F, Chen C and Yang KH. A computational modeling of the biomechanical response of pig head under blast loading. In: Proceedings of 17th U.S. National Congress on Theoretical & Applied Mechanics, June, 2014, East Lansing, MI, USA.

Zhang L, Makawana R, Sharma S, Wang L. (2014) Biomechanical Responses of Human Head and Headform in Blast Exposure. Proceedings of 17th U.S. National Congress on Theoretical and Applied Mechanics.

Conference Oral Presentations

Biomechanical Responses of Human Head and Headform in Blast Exposure. Presented at the 17th U.S. National Congress on Theoretical and Applied Mechanics, East Lansing, MI, June 16, 2014.

Comparison of the Brain Response to Blast Exposure Between a Human Head Model and a Blast Headform Model Using Finite Element Methods. Presented at the 13th international LS-DYNA Users Conference, Dearborn, MI, June 10, 2014.

REFERENCES

Liu MB, Liu GR, Lam KY, Zong Z. Smoothed particle hydrodynamics for numerical simulation of underwater explosion. Computational Mechanics 30:106-118, 2003.

Jin, X; Ma, C; Zhang, L; Yang, KH; King, AI; Dong, G; Zhang, J: Biomechanical response of the bovine pia-arachnoid complex to normal traction loading at varying strain rates. Stapp Car Crash J., 51: 115-126, Paper no. 2007-22-0004, 2007.

Jin, X; Yang, KH, King, AI: Mechanical properties of bovine pia-arachnoid complex in shear. Journal of Biomechanics, 44(3): 467-474, 2011.

Zhang L, Makwana R, Sharma S. Brain response to primary blast wave using validated finite element models of human head and advanced combat helmet. Frontier in Neurology 2013; 4:88. doi: 10.3389/fneur.2013.00088.